ELSEVIER

Contents lists available at ScienceDirect

Brain Stimulation

journal homepage: www.journals.elsevier.com/brain-stimulation





Photoswitching endogenous glutamate receptors in neural ensembles and single synapses *in vivo*

Aida Garrido-Charles ^{a,b,l,5}, Miquel Bosch ^{a,b,m,5}, Hyojung Lee ^{a,b}, Xavier Rovira ^{a,b,1}, Silvia Pittolo ^{a,b}, Artur Llobet ^{c,d,e}, Hovy Ho-Wai Wong ^{f,n}, Ana Trapero ^{a,g,2}, Carlo Matera ^{a,b,3}, Claudio Papotto ^{a,4}, Carme Serra ^g, Amadeu Llebaria ^g, Eduardo Soriano ^{h,i}, Maria V. Sanchez-Vives ^{j,k}, Christine E. Holt ^f, Pau Gorostiza ^{a,b,k,*}

- a Institute for Bioengineering of Catalonia (IBEC), Barcelona Institute for Science and Technology (BIST), Carrer de Baldiri Reixac 15-21, 08028, Barcelona, Spain
- b Network Biomedical Research Center in Bioengineering, Biomaterials, and Nanomedicine (CIBER-BBN), 28029, Madrid, Spain
- ^c Laboratory of Neurobiology, Neuroscience Program, Bellvitge Biomedical Research Institute (IDIBELL), L'Hospitalet de Llobregat, Spain
- d Department of Pathology and Experimental Therapy, School of Medicine, University of Barcelona, L'Hospitalet de Llobregat, Spain
- ^e Institute of Neurosciences, University of Barcelona, L'Hospitalet de Llobregat, Spain
- f Department of Physiology, Development and Neuroscience, University of Cambridge, Cambridge, UK
- 8 Institute of Advanced Chemistry of Catalonia, Consejo Superior de Investigaciones Científicas (IQAC-CSIC), 08034, Barcelona, Spain
- h Department of Cell Biology, Physiology, and Immunology, Institute of Neurosciences, University of Barcelona (UB), 08028, Barcelona, Spain
- i Network Center of Biomedical Research in Neurodegenerative Diseases (CIBERNED), 28031, Madrid, Spain
- ^j Institut d'Investigacions Biomèdiques August Pi i Sunyer (IDIBAPS), Barcelona, Spain
- k Catalan Institution for Research and Advanced Studies (ICREA), 08010, Barcelona, Spain
- ¹ Institute for Cardiovascular Physiology, University Medical Center Göttingen, Humboldtallee 23, 37073, Göttingen, Germany
- ^m Department of Biomedical Sciences, Universitat Internacional de Catalunya (UIC), 08195, Sant Cugat del Vallès, Spain
- ⁿ Gerald Choa Neuroscience Institute & School of Biomedical Sciences, The Chinese University of Hong Kong, Hong Kong, China

ARTICLE INFO

Keywords:
Covalent drug
Azobenzene
Photoswitch
Photopharmacology
Optopharmacology
AMPAR
Kainate
Dendritic spines
Plasticity
Long-term depression
Pulse-chase
Hippocampus
Calcium imaging
Xenopus

Rat

ABSTRACT

Purpose: To interrogate animal physiology *in vivo*, there is a lack of non-genetic methods to control the activity of endogenous proteins with pharmacological and spatiotemporal precision. To address this need, we recently developed targeted covalent photoswitchable (TCP) compounds that enable the remote control of endogenous glutamate receptors (GluRs) using light.

Methods: We combine the photopharmacological effector TCP9 with neuronal activity sensors to demonstrate alloptical reversible control of endogenous GluRs across multiple spatiotemporal scales in rat brain tissue *ex vivo* and in *Xenopus* tadpole brains *in vivo*.

Findings: TCP9 allows photoactivation of neuronal ensembles, individual neurons, and single synapses in *ex vivo* tissue and in intact brain *in vivo*, which is challenging using optogenetics and neurotransmitter uncaging. TCP9 covalently targets AMPA and kainate receptors, maintaining their functionality and photoswitchability for extended periods (>8 h) after a single compound application. This allows tracking endogenous receptor physiology during synaptic plasticity events such as the reduction of functional AMPA receptors during long-term depression in hippocampal neurons.

Conclusion: TCP9 is a unique non-invasive tool for durable labeling, reversible photoswitching, and functional tracking of native receptors in brain tissue without genetic manipulation.

https://doi.org/10.1016/j.brs.2025.09.005

Received 15 April 2025; Received in revised form 6 September 2025; Accepted 7 September 2025 Available online 11 September 2025

1935-861X/© 2025 The Authors. Published by Elsevier Inc. This is an open access article under the CC BY-NC license (http://creativecommons.org/licenses/by-nc/4.0/).

^{*} Corresponding author. Institute for Bioengineering of Catalonia (IBEC), Barcelona Institute for Science and Technology (BIST), Carrer de Baldiri Reixac 15-21, 08028, Barcelona, Spain.

E-mail address: pau@icrea.cat (P. Gorostiza).

¹ Present address: Institute of Advanced Chemistry of Catalonia, Consejo Superior de Investigaciones Científicas (IQAC-CSIC), 08034 Barcelona, Spain.

² Present address: Gain Therapeutics, Spain branch, Parc Científic de Barcelona, 08028 Barcelona, Spain.

³ Department of Pharmaceutical Sciences, University of Milan, Via L. Mangiagalli 25, 20133 Milan, Italy

⁴ Present address: School of Medicine and Surgery, University of Milano-Bicocca, Via Cadore 48, 20900 Monza, Italy.

⁵ These two authors made an equivalent contribution to this work.

1. Introduction

Noninvasive methods to selectively track endogenous proteins and to reversibly control their activity *in vivo* are essential to understand physiology and to regulate them for therapeutic purposes. However, the most widely used molecular tools rely on the genetic introduction of exogenous proteins or conventional non-regulatable pharmacology. There is a lack of robust methods to monitor and regulate the activity of endogenous proteins selectively and with spatiotemporal precision without genetic manipulation. This need is especially compelling at the level of single synapses, due to their small size and their potential as therapeutic targets in neuropathology.

Glutamate receptors (GluRs) play an essential role in neuronal physiology. They are responsible for the transmission of electrochemical signals and the regulation of the plastic properties of excitatory synapses [1]. Ionotropic GluRs are cation-permeable ion channels that open upon glutamate binding and contribute to the depolarization of the postneuron. them. synaptic Among the α-amino-3-hydroxy-5-methyl-4-isoxazolepropionic acid (AMPA)-type (AMPAR), the kainate-type (KAR), and the N-methyl-D-aspartic acid (NMDA)-type (NMDAR) are the most important [2]. AMPARs and KARs provide the main contribution to synaptic transmission as their density in the postsynaptic membrane determines the strength of the synapse. NMDARs are mainly responsible for regulating synaptic plasticity, primarily via Ca²⁺ entry, which triggers long-term potentiation (LTP) or long-term depression (LTD) [3] of synaptic transmission.

Studying and manipulating GluRs has been a long-standing quest in neurobiology. The turn-over and dynamics of GluRs between the synapse, extrasynaptic regions, and internal membranes during the basal state and plasticity events have been extensively investigated using diverse methods [4-7]. Biochemical tools, such as biotinylation [8,9], radioisotope or heavy isotope labeling [10-12] allow the quantification of endogenous GluRs but are not well suited for longitudinal and real-time monitoring. The development of optical and photochemical tools, such as the fusion with fluorescent proteins (e.g. EGFP [13]) or modifiable-fluorescence proteins (e.g. super ecliptic pHluorin [14,15], or photoactivatable GFP [16]) allow localization tracking of GluRs over time using confocal, two-photon, super-resolution or single particle/molecule tracking microscopy techniques [5]. However, these approaches require genetic engineering and/or overexpression of exogenous proteins. These limitations also apply to alternative labeling methods such as SNAP-tag [17], Halotag [18], small peptides [19], unnatural amino acids [11,20,21], electrophysiological [22] or immunoreactive tags [23,24]. Knock-in approaches permit the detection of endogenous GluRs, avoiding overexpression issues but still require genetic manipulation [25–27]. These research approaches are sometimes prohibitive because of time and resource limitations. Recently developed ligand-directed chemical methods [28,29] achieve the non-genetic labeling of endogenous GluRs but cannot detect whether the receptors are functional. Thus, none of these observation methods combines the requirements of longitudinal, real-time tracking of functional, endogenous GluRs.

For both fundamental research and therapeutic purposes, the manipulation of GluRs has been largely based on pharmacological ligands. The main limitation of conventional pharmacology is its low spatiotemporal resolution, which blurs drug action in basic experiments and causes adverse effects in medical treatments. The development of light-regulated tools has revolutionized the control of neuronal physiology. Two main approaches are used to photocontrol biological processes. The first is optogenetics [30] that is based on the overexpression of intrinsically light-regulated proteins (e.g., Channelrhodopsin-2). The second is photopharmacology [31], which relies on the chemical design of (1) caged drugs that are irreversibly photoreleased, or (2) photoswitchable drugs that toggle between active and inactive configurations. Caged compounds are useful in brain slices but pose challenges for repetitive use *in vivo* with minimal intervention. Two classes of

photoswitchable compounds have been developed: photochromic ligands (PCLs) that diffuse freely in solution, and photoswitchable tethered ligands (PTLs) [32] that are covalently attached to their target receptor. Most PTLs are based on genetically introduced cysteines [31] or tags, such as photoswitchable orthogonal remotely tethered ligands (PORTLs) [33–36]. These tethered photoswitches are valuable tools not only for remotely controlling biological processes but also for molecular mechanism discoveries [37]. For example, they have been used to study GluR desensitization and occupancy [38], working memory mediated by G protein-coupled receptors [39], and the mechanism of GABA_B receptor signaling [40].

However, both optogenetics and tethered photopharmacology require genetic manipulation to overexpress exogenous proteins, tags or amino acids. These can trigger immune responses and disrupt cellular physiology, particularly in small compartments like dendritic spines. A promising alternative approach is offered by targeted covalent photoswitches (TCPs) [41–43], which enable the control of endogenous receptors without genetic manipulation. TCPs are a class of PTLs that use an electrophilic reactive group to covalently conjugate to nucleophilic side chains like lysines, which are abundant in proteins. This approach targets receptors by affinity labeling and does not need genetically introduced cysteines or tags. In this line, we recently developed a class of TCPs that reversibly activate and deactivate endogenous GluRs with light [43,44]. We used them to photocontrol neuronal activity, including endowing light sensitivity to degenerated retina *ex vivo* (TCP9) [43], and to spiral ganglion neurons of the cochlea *in vivo* (TCPfast) [44].

In this study, we push the boundaries of non-genetic tethered photoswitches by employing TCP9 to label GluRs in vitro and in vivo, to control neuronal activity and to investigate endogenous receptor physiology. We put the temporal and spatial resolution of TCPs to the test in preparations of increasing physiological relevance: (1) in vitro dissociated rat hippocampal neuronal cultures, (2) ex vivo rat hippocampal organotypic slices, and (3) in vivo Xenopus olfactory bulb. TCP9 enabled specific, reversible, and remote photocontrol of neuronal ensembles, individual neurons, and single synapses in all cases, including in the intact brain. Furthermore, TCP9 conjugation allowed us to longitudinally monitor the dynamics of functional endogenous GluRs in real-time in events of synaptic plasticity, such as the induction of LTD. Together, these demonstrate that TCP9 is a convenient and effective photopharmacological tool in a broad range of biological systems. This approach provides a blueprint for non-invasive and reversible control of other endogenous receptors in the brain, opening new research avenues in both health and disease.

2. Results

2.1. Targeted covalent photoswitches (TCPs) enable the light-controlled modulation of endogenous glutamate receptor activity in neurons

In order to remotely control the activation and deactivation of endogenous GluRs with light (Fig. 1a), we developed several photoswitchable ligands able to conjugate to these receptors without genetic modifications [43]. We selected TCP9 as one of the most effective photoswitches from this molecular library. TCP9 consists of a glutamate moiety (blue in Fig. 1a–b) linked to the photoisomerizable azobenzene group (green in Fig. 1a–b), which is in turn linked to a highly reactive N-hydroxysuccinimide (NHS) ester group (red in Fig. 1a–b). This design allows TCP9 to attach to endogenous receptors through an affinity labeling process: the glutamate moiety first binds with high affinity to the glutamate pocket of the ligand binding domain (LBD) of the receptor, thereby positioning the NHS group to react with neighboring nucleophilic lysine residues.

TCP9 can adopt two conformations: the azobenzene moiety can be isomerized to the *cis* form by UV-violet light (360–410 nm) and to the *trans* stable form by blue-green light (430–550 nm). The *cis* isomer can also back-isomerize to the *trans* isomer by thermal relaxation in the dark

with a lifetime of ~ 80 min. In the *cis* isoform, TCP9 adopts a bent configuration that positions the glutamate moiety into the glutamate pocket site, producing a full agonist effect that opens the GluR ion channel. In the *trans* isoform, TCP9 adopts an extended configuration that displaces the glutamate moiety and favors the channel closing (Fig. 1a) [43].

We previously demonstrated that TCP9 can light-regulate heterologously expressed GluK1-homotetrameric receptors and endogenous GluRs of dorsal root ganglion and retinal neuronal cultures in vitro [43]. In the present study, we aimed to test the limits of the spatiotemporal resolution of TCP9 in controlling the function of native GluRs in several in vitro and in vivo preparations. We started with dissociated rat hippocampal neurons in two-dimensional (2D) cultures and tested whether the neuronal firing rate could be remotely controlled with light (Fig. 1c-f). TCP9 was prepared before each experiment by click reaction of its two components: the part bearing the azobenzene and glutamate moieties, and the part bearing the reactive anchoring moiety [43]. Neuronal cultures were then incubated with TCP9 for 2 min and immediately washed out. The firing rate of single neurons was measured by patch clamp electrophysiological recordings. We illuminated neurons with flashes of 40 ms of violet light at different frequencies: 1 Hz (Fig. 1c), 5 Hz (Fig. 1d) and 10 Hz (Fig. 1e), alternating with continuous illumination with green light. Violet light pulses robustly triggered action potentials (APs) at the desired frequency (spike probability and amplitude at different frequencies and pulse durations are quantified in Fig. S1). APs were blocked by the application of the competitive AMPAR/KAR antagonists DNQX (Fig. 1f-S1c-d) and NBQX (Fig. S2a), demonstrating that TCP9 is covalently conjugated and acts on AMPARs and/or KARs. Application of AP5 did not block photocurrents (Fig. S2b), suggesting that TCP9 does not influence NMDAR activity. The magnitude of the inward currents in neurons was proportional to the light intensity (Fig. S3).

2.2. TCP9 enables the long-term photocontrol of endogenous GluRs in ex vivo brain tissue

We next tested TCP9 in a developed brain tissue with natural 3D complexity under more physiological conditions. We prepared rat hippocampal organotypic slice cultures, where neurons and synapses maintain similar morphology and physiology to those in the intact brain [45]. We monitored neuronal and synaptic activity over time using fluorescence calcium imaging while simultaneously photoswitching TCP9 with the same confocal microscope [46,47]. This all-optical approach allowed us to combine optical effectors (TCP) with optical sensors (chemical or genetically encoded calcium indicators) to monitor multiple cells at the same time. We biolistically transfected neurons with plasmids expressing the calcium sensor GCaMP6s together with DsRed2 (Fig. 2a). We used DsRed2 both as a cell filler to locate neurons and spines and as calcium-independent fluorescence control signal. We incubated slices in TCP9 for 15 min, washed it out, and performed time-lapse live imaging under continuous perfusion of carbogenated artificial cerebrospinal fluid (ACSF) at room temperature. To induce the cis isomerization of TCP9 in all conjugated cells, we raster-illuminated the entire field of view with the violet light laser (405 nm) for 1 min. About half of the DsRed2-transfected neurons (average of 48.4 \pm 3.0 % per experiment, 83 out of 170 cells from 14 experiments) responded with an increase in GCaMP6s fluorescence upon violet illumination (considered positive photoresponse if > 50 % over baseline, Fig. 2b-d). We back-isomerized TCP9 to the trans isoform by raster-scanning the green laser (514 nm) for another minute. Most of the cells (89.6 \pm 4.6 %

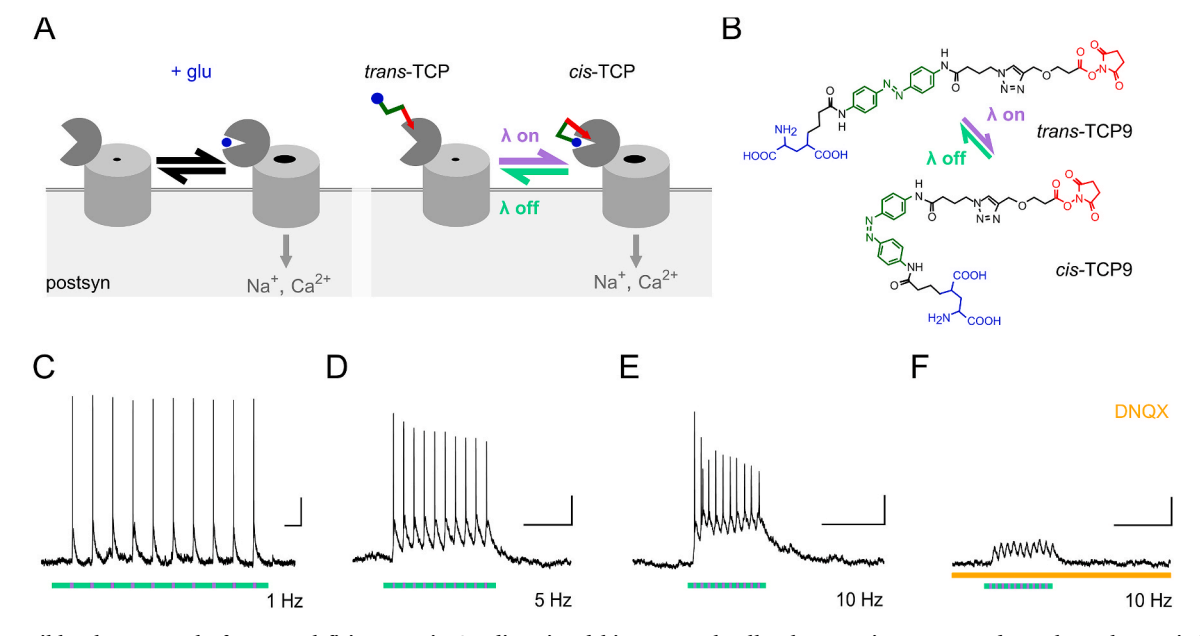


Fig. 1. Reversible photocontrol of neuronal firing rate in 2D dissociated hippocampal cell cultures using a targeted covalent photoswitch (TCP) of endogenous glutamate receptors. a) Operational mode of TCP9 on GluRs [43]. In physiological conditions (left), glutamate secreted by presynaptic terminals binds to the extracellular ligand binding domain (LBD) of GluRs at the postsynaptic membrane and opens their cation-permeable channel. The TCP9 photoswitchable tethered agonist exerts an equivalent effect on GluRs (right). The glutamate moiety (blue dot) is tethered to the LBD through a reactive NHS ester group (red line) *via* a reversibly photoswitchable azobenzene group (green line). In the *trans* state of the switch, glutamate cannot reach the ligand binding pocket, whereas in the *cis* state, the glutamate moiety can bind and activate the receptor, opening the channel pore and depolarizing the postsynaptic terminal. Switching between *cis* and *trans* states is achieved by illumination with violet and green light, respectively. b) TCP9 chemical structure showing the photoisomerization between the *trans* configuration (promoted by green light, $\lambda = 430-550$ nm, or thermal relaxation in the dark) and the *cis* configuration (promoted by violet light, $\lambda = 360-410$ nm). c-f) Representative current clamp recordings from a rat hippocampal neuron (membrane potential set at -70 mV) after 11 days in culture, treated with 12.4 μ M TCP9 for 2 min at pH 9, washed, and exposed to alternating 500 nm (green rectangles) and 380 nm (violet rectangles) light pulses. Violet light pulses of 40 ms and 0.8 mW cm⁻² were delivered at 1 Hz (c), 5 Hz (d) and 10 Hz (e) in the same neuron. (f) Photoresponses in this neuron are inhibited in the presence of 1 mM DNQX (AMPAR/KAR antagonist, orange bar). Scale bars represent 10 mV, 1 s. Quantification of the photostimulation parameters of panels c-f across different neurons and pulse durations is shown in Fig. S1.

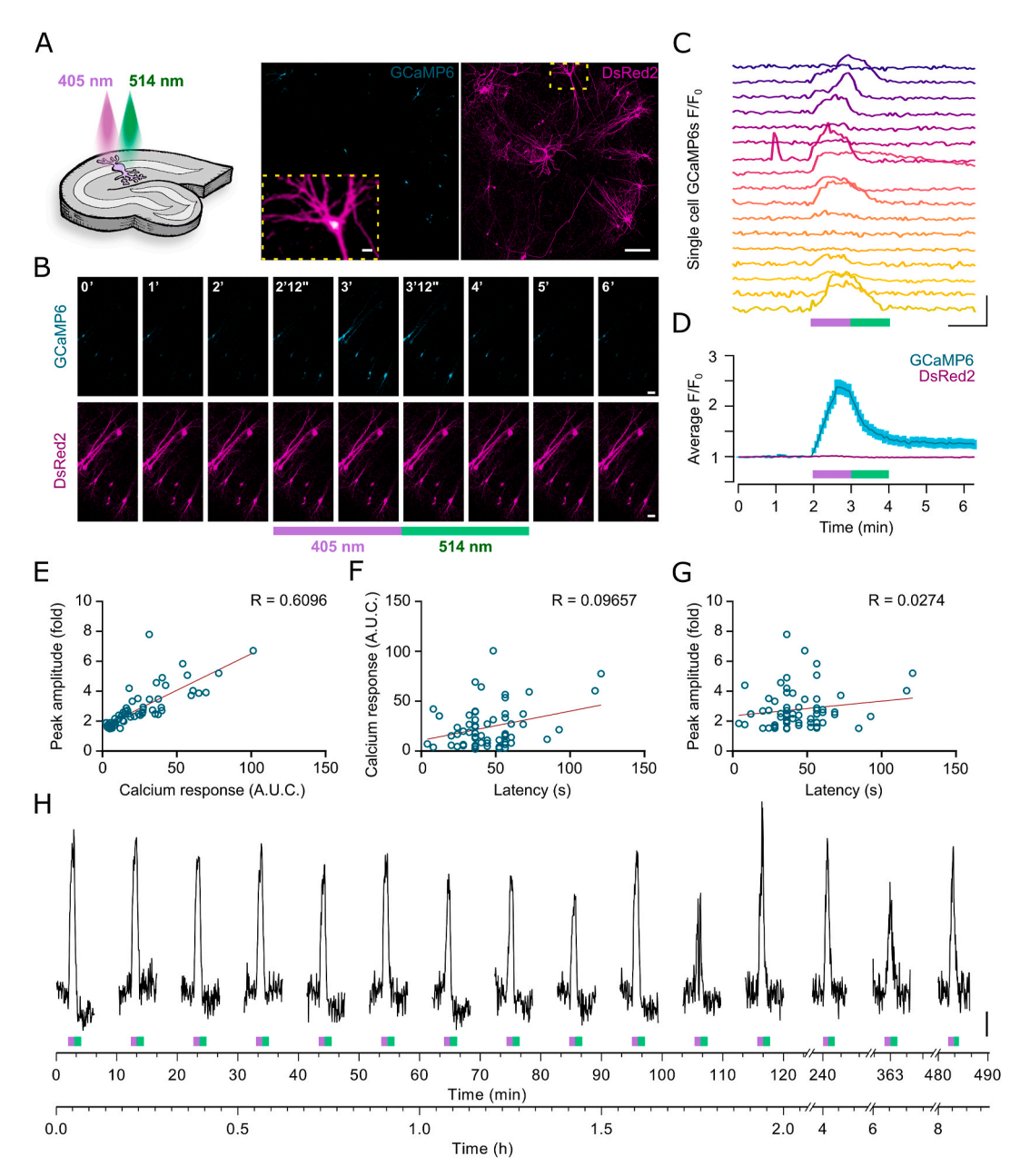


Fig. 2. TCP9 permits the long-term reversible photocontrol of neuronal activity in 3D organotypic hippocampal slices mediated by endogenous GluRs. a) Schematic drawing of a rat organotypic hippocampal slice culture, and microphotographs of a slice expressing GCaMP6s (cyan) and DsRed2 (magenta). Inset image corresponds to the GCaMP6 and DsRed2 superposition of the neuron in the yellow square. Scale bars represent 200 μ m, and 20 μ m for the inset. b-d) All-optical approach allows simultaneous activity sensing (GCaMP6s imaging) and activity regulation (TCP9 photoswitching). b) Time-lapse images of GCaMP6s and DsRed2 fluorescence after incubation in 250 μ m TCP9 for 15 min at pH 7.4, showing an increase and a decrease in GCaMP6s fluorescence during sequential illumination with 405 nm and 514 nm light, respectively. Scale bar, 50 μ m. c) Time course of GCaMP6s signals from 17 individual cells from the slice shown in (a), stimulated with a 405 nm raster scanning laser (violet bar, 1 min, 0.81 mW μ m⁻²) to activate TCP9, followed by 514 nm laser scanning stimulation to deactivate TCP9 (green bar, 1 min, 0.35 mW μ m⁻²). Scale bars indicate two-fold increase (F/F₀) and 1 min. d) Time course of acreaged GCaMP6s and DsRed2 signals normalized to baseline (F/F₀) upon light stimulation (405 and 514 nm). Data represented as mean \pm SEM of n = 65 photoresponsive cells from 12 slices. e-g) Correlation between e) calcium peak amplitude (fold over baseline) and calcium response magnitude (area under the curve, AUC, of the violet and green stimulation period, in arbitrary units); f) calcium response magnitude (AUC) and peak latency (from light onset to peak); and g) peak amplitude and peak latency, from n = 65 photoresponsive cells. h) Slices incubated for 2 min in TCP9 and maintained for several hours under the microscope show sustained Ca²⁺ photoresponses after repeated illumination patterns (same violet and green light pulses as in b-d), up to ~8 h (482 min). Traces are GCaMP6s mean signal of n = 10 photoresp

per experiment, 73 out of 83 responsive cells from 14 experiments) ceased their activity after green light exposure. On average, cells responded to TCP9 activation with a 2.76 \pm 0.16 -fold increase in GCaMP6s signal over baseline at the maximum peak, and with a peak latency (from stimulus onset to peak) of 44.1 \pm 2.6 s (Fig. 2c–d). The area under the curve (AUC) of the integrated GCaMP6s signal (measured

from the onset of the violet light until the end of the green illumination), as a quantification of the overall magnitude (amplitude + duration) of the photoresponse, was 23.7 ± 2.6 (in arbitrary units, for comparison with subsequent experiments). We found a correlation between the peak amplitude and the photoresponse AUC (R = 0.61, Fig. 2e), but no correlation between the photoresponse AUC and the peak latency (R =

0.10, Fig. 2f) or between the peak amplitude and the peak latency (R = 0.03, Fig. 2g). Control experiments with transfected slices but not incubated with TCP9 showed some spontaneous neuronal activity but no correlated responses to the photostimulation (see Fig. 3f–g).

Given the thickness of the slice, we were initially concerned that TCP9 would react only with the slice surface and not with cells in deeper layers. However, we found cells responding to violet light at depths from 20 μ m down to 145 μ m (Fig. S4), indicating that TCP9 efficiently penetrates deep into the tissue. Notably, photoresponses were quantitatively maintained for >8 h after TCP9 incubation in the same population of neurons without evidence of photobleaching or photo-fatigue (Fig. 2h). Such persistence allows long-term experiments on GluR dynamics, including pharmacological profiling and tracking receptor activity during events of neuronal plasticity (see Fig. 4).

We next characterized TCP9-evoked photoresponses pharmacologically, taking advantage of our all-optical ability to simultaneously stimulate and record a large population of neurons in organotypic slices (Fig. 3). Compared to control conditions (Fig. 3a), bath perfusion of TTX (Na⁺ channel blocker, Fig. 3b) did not affect the photoresponse amplitude, suggesting that TCP9 acts postsynaptically (including dendrites and soma) and does not require presynaptic glutamate release. Similarly, perfusion of AP5 (NMDAR antagonist, Fig. 3c) did not block the photoresponse, suggesting that TCP9's effects are not mediated by NMDARs. In contrast, photoresponses were largely reduced by NBQX and CNQX (both AMPAR and KAR antagonists) (Fig. 3d-e), consistent with our results from dissociated hippocampal neuron cultures using DNQX and NBQX (Fig. 1f-S1c-d, S2a). Photostimulation in the absence of TCP9 did not elicit calcium responses (Fig. 3f). These results demonstrate that TCP9 photoactivation in hippocampal slices is mainly mediated by postsynaptic AMPARs and/or KARs (Fig. 3g).

2.3. Functional tracking of endogenous GluRs during events of synaptic plasticity

After characterizing the abilities of TCP9 to photocontrol endogenous GluRs in brain tissue, we next applied TCP9 to study synaptic plasticity phenomena in an unexplored way. We utilized TCP9-evoked photoresponses to continuously report the presence of functional endogenous AMPARs/KARs in neuronal membranes. The stability of these photoresponses (lasting up to ~ 8 h) allowed us to monitor

dynamic changes in receptor functionality over time. We here used TCP9 to track the internalization of functional AMPARs during the induction of long-term depression (LTD) of synaptic transmission in hippocampal neurons [48,49].

We incubated organotypic hippocampal slice cultures with TCP9 for 15 min and, using the all-optical approach of Figs. 2 and 3, we monitored calcium photoresponses every 20 min for 2 h (Fig. 4). We then induced NMDAR-dependent LTD by applying 20 µM NMDA for 3 min. The average amplitude of TCP9-evoked photoresponses decreased by \sim half within 5 min of NMDA application and remained significantly lower $(-25.1 \pm 9.2 \%)$ for the next 2 h (Fig. 4a–c), as previously reported [50]. The all-optical approach allowed us to photostimulate and record calcium responses from individual neurons in the slice (Fig. 4b). Most of them showed a decrease in amplitude and/or duration of photoresponses after NMDA application. Thus, TCP9 conjugation and photoswitching permits not only monitoring endogenous receptors longitudinally (which is difficult with other live methods based on exogenous proteins that might interfere with endogenous protein dynamics) but also revealing the receptors that are functional at the plasma membrane (i.e., that produce intracellular calcium responses upon photoactivation). This is a novel and comprehensive way to monitor GluR functionality in naïve conditions, without genetic manipulation.

2.4. TCPs can optically activate single neurons and single synapses in ex vivo brain tissue

We followed by testing the limits of the spatiotemporal resolution of TCP9-mediated photocontrol of neuronal activity (Fig. 5). After using whole-field raster illumination to photoactivate the hippocampal slice in previous experiments, we next targeted individual neurons by focusing the violet (405 nm) laser beam on the soma of pyramidal neurons of the CA1-CA3 region of the hippocampus. We illuminated each neuron for 10-20 s (Fig. 5a–b) and observed an increase in calcium fluorescence in the soma, similar in amplitude of response (3.1 \pm 0.4 -fold) and overall magnitude (GCaMP6s signal AUC of 24.8 ± 7.5 in arbitrary units, Fig. S5c–d) to whole-field illumination experiments, but with faster response latency (10.0 ± 2.6 s, Fig. S5e and g), and constrained to the targeted cell (Fig. 5b–c). Occasionally, we observed an increase in calcium signal in cells not directly illuminated by our laser, with a delay of seconds (e.g. Fig. 5b right panel). This could be due to dendrites from

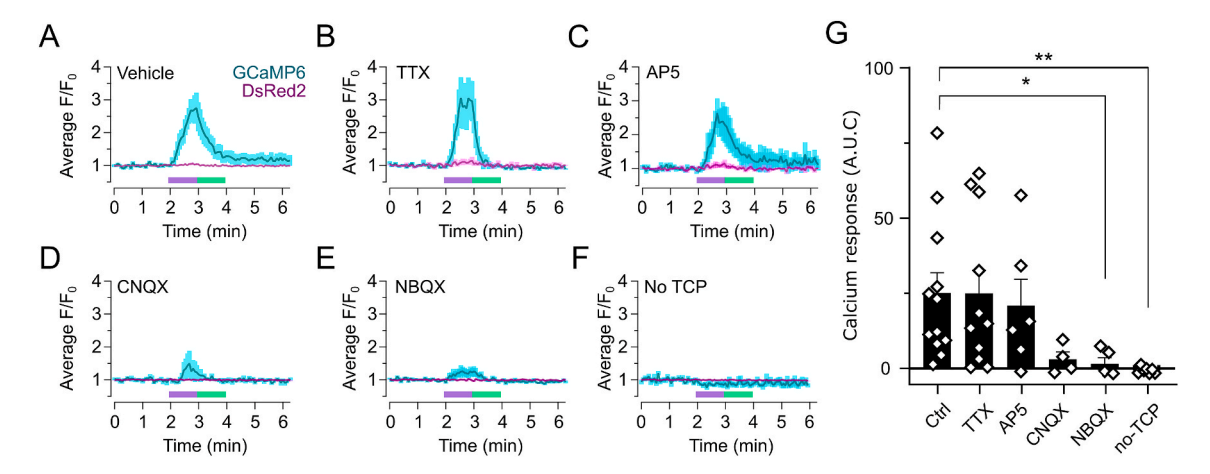


Fig. 3. The photoswitchable action of TCP9 on neuronal activity is mediated by postsynaptic endogenous AMPA and KA GluRs. To identify the target receptor of TCP9, light-evoked calcium responses in organotypic rat hippocampal slices were recorded in the presence of several pharmacological treatments. a-f) Average fluorescence intensity of GCaMP6s (cyan) and DsRed2 (magenta) signals over time, normalized to baseline (F/F₀), before, during, and after light stimulation (405 nm, violet bars; 514 nm, green bars) in a) control (vehicle) conditions, b) in the presence of 1 μ M of the sodium channel blocker TTX, c) 100 μ M of the NMDAR antagonist AP5, d) 10 μ M of the AMPAR/KAR antagonists CNQX, and e) NBQX, and f) without TCP9 incubation. g) Quantification of overall photoresponses measured as area under the curve (AUC) of integrated GCaMP6s fluorescence intensity signals. Significant inhibition of calcium responses is observed for NBQX, demonstrating that endogenous AMPARs and/or KARs primarily mediate TCP9 neuronal photoresponses. Data are represented as mean \pm SEM (n = cells from different slices): Vehicle, n = 12; TTX, n = 11; AP5, n = 6; CNQX, n = 4; NBQX, n = 5; no TCP9, n = 6. *p < 0.05, **p < 0.01 with respect to vehicle control (Kruskal-Wallis test with Dunn's multiple comparison test).

Brain Stimulation 18 (2025) 1779-1793

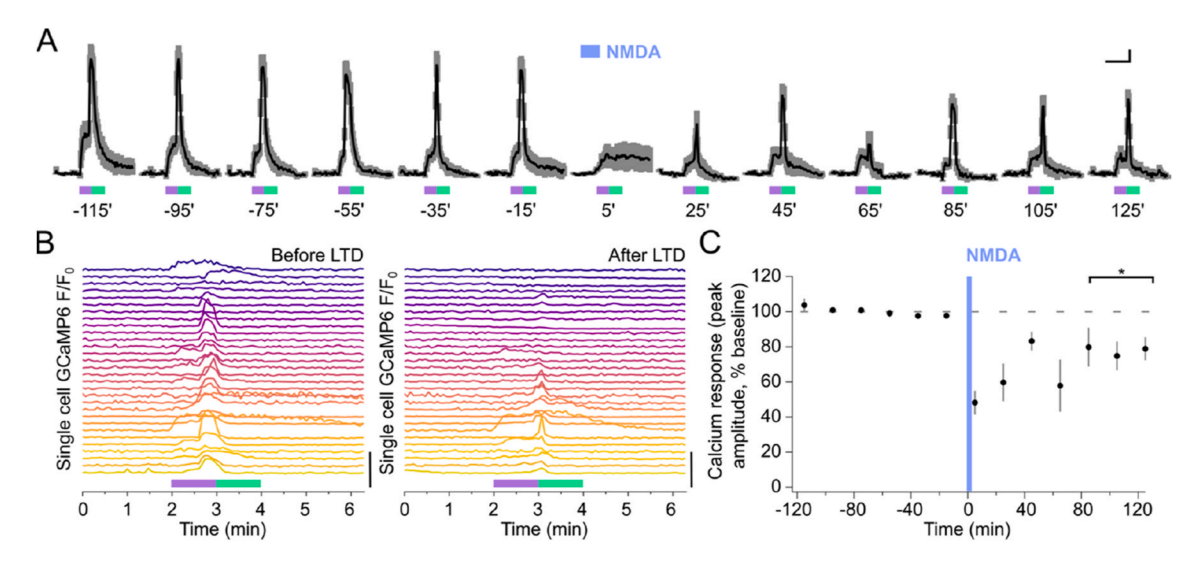


Fig. 4. TCP9 allows tracking functional endogenous AMPA/KA GluRs during the induction of long-term depression. a) Cycles of photostimulation (violet rectangles, 1 min) and photodeactivation (green rectangles, 1 min) of TCP-conjugated cells in organotypic hippocampal slices were repeated every 20 min for 4 h. Each time point represents the beginning of the 6-min time-course of the GCaMP6s mean fluorescence signal \pm SEM of n=10 cells from one representative experiment. Baseline photoresponses were stable for 2 h. Bath perfusion with 20 μ M NMDA for 3 min (at time 0, blue square) reduced the magnitude of subsequent photoresponses for at least 125 min, confirming the induction of long-term depression (LTD). Scale bars represent 0.3-fold (F/F₀) and 2 min. b) GCaMP6s fluorescence traces corresponding to individual neurons are shown before (-15 min) and after (25 min) NMDA application (n=30 neurons from 4 slices). Scale bar indicates 10-fold increase (F/F₀). c) Average of GCaMP6s peak amplitude photoresponses normalized to baseline (F/F₀) over time shows a long-term decrease in photoresponse intensity of 25 % (mean \pm SEM of n=4 independent slices). *p < 0.05 comparing the last 60 min period (85'-125') with the 60 min baseline period before application of NMDA (Student's paired t-test).

these non-illuminated cells being unknowingly present in the illuminated region, or due to the synaptic connectivity between both neurons. This observation reveals an interesting application of TCPs: the characterization of the connectivity in genetically unaltered neural circuits, which will be the object of a dedicated study. In control experiments, we did not detect any increment in GCaMP6s signal in the neuronal soma of TCP-non conjugated slices after single cell illumination (Fig. S5a).

We next aimed at using TCP9 to photocontrol single synapses, which are submicrometer-sized compartments lying at the limit of spatial resolution of conventional optical microscopy (Fig. 5d-f). To do this, we selected DsRed2+GCaMP6s-transfected neurons in hippocampal slices and confirmed that they were efficiently conjugated with TCP9 by testing their positive response to illumination at the soma. We then zoomed-in on individual dendritic spines located at the distal region of secondary apical dendrites. We focused the 405 nm laser beam near the tip of the selected spine (Fig. 5d) and illuminated it with 1 s pulses. We detected synchronized GCaMP6s fluorescence peaks within the spine head right after the 405 nm pulse. The latency from light pulse to peak response was 1-2 s (1-2 frames) with TCP9, with a mean response amplitude of 1.64 \pm 0.11 -fold over baseline (Fig. 5d–f, S5c-f, h). The GCaMP6s peak signals in control experiments without TCP9 conjugation were randomly distributed and not synchronized with light stimulation (Fig. S5b and h), ruling out the possibilities of direct photoactivation and/or artefactual responses due to photodamage. We did not detect significant changes in the DsRed2 signal, ruling out the possibility of cross-bleeding between channels or photobleaching. We occasionally observed an increment of the GCaMP6s signal in the dendritic compartment adjacent to the stimulated spines, but TCP9-evoked responses were usually confined to the spine head compartment (Fig. S6). Remarkably, photoactivation of the same individual spine could be achieved repeatedly over time (Fig. 5e). Taken together, our experiments in hippocampal slices demonstrate that TCP9 enables photocontrol of neuronal activity via endogenous GluRs without genetic manipulation across several spatiotemporal scales, from neuronal ensembles with a time frame of minutes, to individual neurons, and down to single synapses at the micrometer and second scales.

2.5. TCP9 allows photocontrolling the activity of single neurons and single synapses in vivo

The robust photocontrol of neural activity in organotypic brain slices provided by TCP9 encouraged us to test its efficacy *in vivo* in the intact brain. We selected *Xenopus* larvae as a suitable animal model because their translucent skin allows for easy illumination and fluorescence readout [51–53]. Furthermore, *Xenopus* larvae are simple to manipulate, can be obtained in large numbers, and possess a small but complex nervous system. This allows illuminating the entire brain while recording the activity from single neurons. In addition, certain olfactory bulb (OB) neurons feature dendritic spines, providing a unique opportunity to study single synapses *in vivo* without needing the complex procedures required in higher vertebrates [54].

Although GluRs are highly conserved across animal kingdoms, we initially tested whether the amphibian Xenopus neurons were amenable to photoswitching with TCP9 (Fig. S7) as shown in mammalian neurons (Figs. 1–5). We started by preparing ex vivo acute slices of the Xenopus telencephalon and incubating them with TCP9 for 15 min. For simplicity, we used the chemical calcium sensor Oregon Green BAPTA (OGB-1) to record evoked photoresponses after TCP9 conjugation (Figs. S7a, c, e-f) and spontaneous neuronal activity (Figure S7b, g-h). Whole-field illumination with 380 nm light followed by 500 nm light (Fig. S7a and c) triggered calcium responses in TCP-conjugated slices that were ~50 % of those obtained after application of 1 mM glutamate (Fig. S7d, quantified in Fig. S8). Illumination with 380 nm light alone (Fig. S7e) or preceded by 500 nm light (Fig. S7f) also triggered calcium responses, confirming that green light is not required to switch off TCP9 because of continuous scanning with 488 nm imaging laser. In control experiments, calcium responses were neither observed by 380 nm and 500 nm stimulation of non-conjugated slices (Fig. S7h-i) nor by 500 nm alone stimulation of TCP9-conjugated slices (Fig. S7j).

Once the efficacy of TCP9 in *Xenopus* slices was confirmed, we moved to testing it in the intact brain *in vivo*. We electroporated *Xenopus laevis* embryos with plasmids expressing the calcium indicator GCaMP6s and the red fluorescent protein mRFP as a morphological marker. We electroporated laterally in one OB and part of the optic tectum (OT)

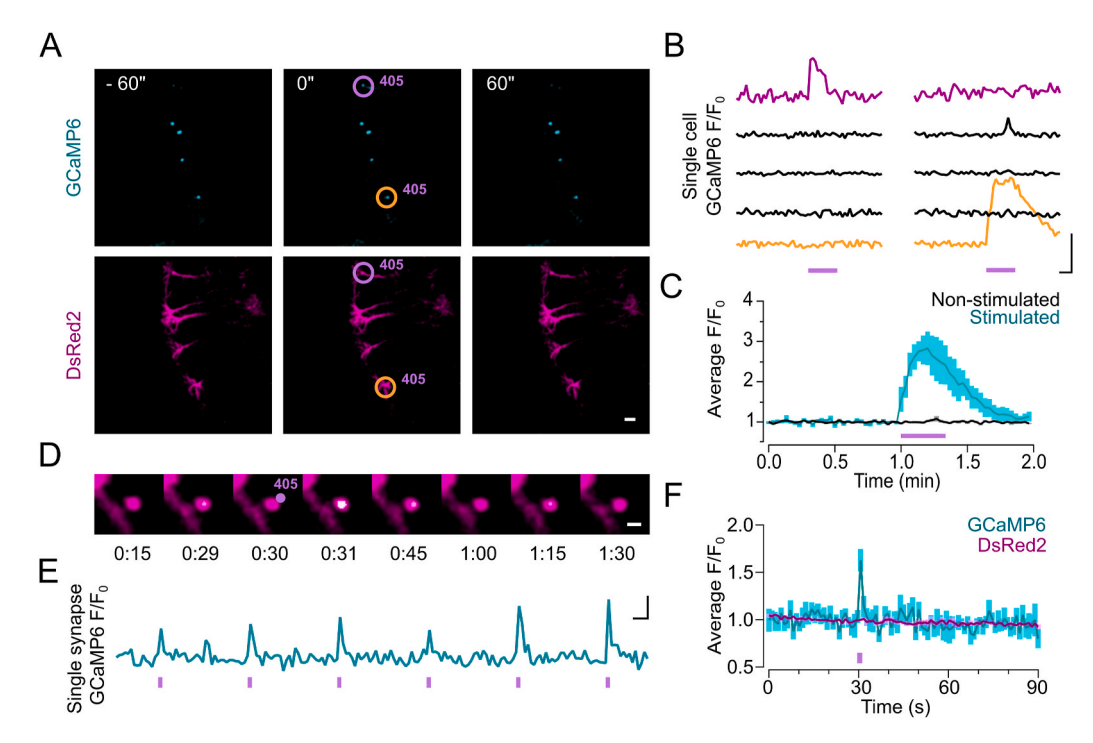


Fig. 5. TCP9 enables robust, rapid, and reversible photocontrol of single-neuron and single-synapse activity in organotypic hippocampal slices. a) Time-lapse images of GCaMP6s (cyan) and DsRed2 (magenta) fluorescence of TCP9-evoked photoresponses on single neurons (purple circle cell photoactivated). Scale bar corresponds to 50 μ m. Time in seconds. b) GCaMP6s signals from 5 single cells in the field of view in (a) after illumination for 20 s (purple bar) with a spotlight of 405 nm laser (0.81 mW μ m⁻²) on the soma (top trace corresponds to the cell circled in purple, and bottom trace to the cell circled in orange) photoactivated in two sequential experiments. Scale bars represent 5-fold (F/F₀) and 10 s. Note that green light is not required to switch off TCP9 because of continuous scanning with 488 nm imaging laser. c) Average GCaMP6s signal in the soma (mean \pm SEM) normalized to baseline (F/F₀) of stimulated cells (cyan, n = 6 cells from 5 slices) and non-stimulated neighboring cells (black, n = 12 cells from 5 slices), upon light stimulation of a single cell (20 s, purple rectangle). d) Time-lapse images of merged fluorescence signals from GCaMP6s (cyan) and DsRed2 (magenta) showing a TCP9-evoked photoresponse in a single spine. The 405 nm laser targeted a spot close to the tip of the spine head (purple dot) for 1 s. Time stamps are in min:sec. Scale bar 1 μ m. e) Time course of GCaMP6s signal (F/F₀) of a single spine repeatedly photostimulated with pulses of the 405 nm laser (1 s, 0.25 mW μ m⁻², purple rectangles) at the tip of the same spine. Scale bars represent 0.5-fold (F/F₀) and 5 s. f) Average fluorescence signal of GCaMP6s and DsRed2 in the spine head (mean \pm SEM) normalized to baseline (F/F₀) upon light stimulation of a single spine (1 s, purple rectangle, n = 5 spines from 5 slices). Photoresponse parameters (peak amplitude, latency and AUC) of single cells and single spines in TCP conjugated and non-conjugated slices are compared in Fig. S5.

(Fig. 6a-c) [55,56]. Around 5-8 days later, we incubated the tadpole in a solution containing TCP9 for 15 min. Using the all-optical method applied in rat brain slices (Figs. 2-5), we recorded neural activity in single or multiple neurons via calcium imaging while photostimulating one or many neurons in vivo (Fig. 6). We observed spontaneous activity in transfected neurons incubated with TCP9 prior to any photostimulation (Fig. 6d bottom, S7b) that was comparable to the spontaneous activity without TCP9 (Fig. 6d top, S7g), which suggests that TCP9 does not interfere with normal neural physiology in these conditions. We then illuminated the whole field for 50 ms with the 405 nm laser and observed synchronized evoked calcium responses in multiple neurons (Fig. 6e), that were reliably produced after several repeated photostimulations onto the same neuronal ensemble. These photoresponses were absent in TCP-non incubated tadpoles (Fig. 6f). We next aimed at photocontrolling single neurons in vivo. We illuminated the soma of individual OB neurons with a spot for 500 ms of the 405 nm laser (Fig. 6g) and observed evoked calcium responses that were synchronized to the light pulse and largely constrained to the stimulated cell (Fig. 6h-i). In contrast, TCP-non incubated tadpoles did not show synchronized photoresponses (Fig. 6j).

To further explore the limits of TCP9-mediated photosensitivity, we finally aimed to reach the finest spatiotemporal resolution possible of light-mediated control of neuronal activity *in vivo*: the single dendritic spine. The OB is the only region described to have neurons with dendritic spines in *Xenopus* [54]. We localized spines in mRFP-expressing OB neurons (Fig. 7a) and pointed the 405 nm laser beam next to the tip of these spines. We switched the laser on for 500 ms while recording

the GCaMP6s fluorescence and observed an evoked increase in the calcium signal within the targeted spine (Fig. 7a-b). Remarkably, the same spine could be reliably photostimulated multiple times, and the evoked calcium responses were reproducible (Fig. 7c). The mRFP signal did not show abrupt changes, ruling out artefactual cross-bleeding. Control experiments in electroporated tadpoles that were not conjugated with TCP9 did not elicit comparable calcium signal increases after 405 nm laser photostimulation in single spines, even at higher light power (Fig. 7d-e), ruling out artifact-induced photoresponses. In general, TCP9 photoresponses evoked in vivo were comparable to those obtained in organotypic hippocampal slices in terms of reproducibility, recovery time, spatial confinement, and time resolution. Altogether, our experiments demonstrate that TCP9 is an effective non-genetic chemical tool to control neuronal activity via endogenous GluRs, capable of reaching single-synapse precision with millisecond light pulses, across in vitro, ex vivo, and in vivo systems.

3. Discussion

Targeted covalent photoswitches (TCPs) were developed to permanently attach to glutamate receptors, thereby enabling control of the opening and closing of their cation pores using specific light wavelengths [43]. This confers TCPs the ability to regulate neuronal activity in a remote and reversible manner. In this work, we have explored the capabilities of TCP9 to photocontrol endogenous GluRs in the brain at different spatiotemporal scales.

The distinctive properties of TCP9 complement those offered by

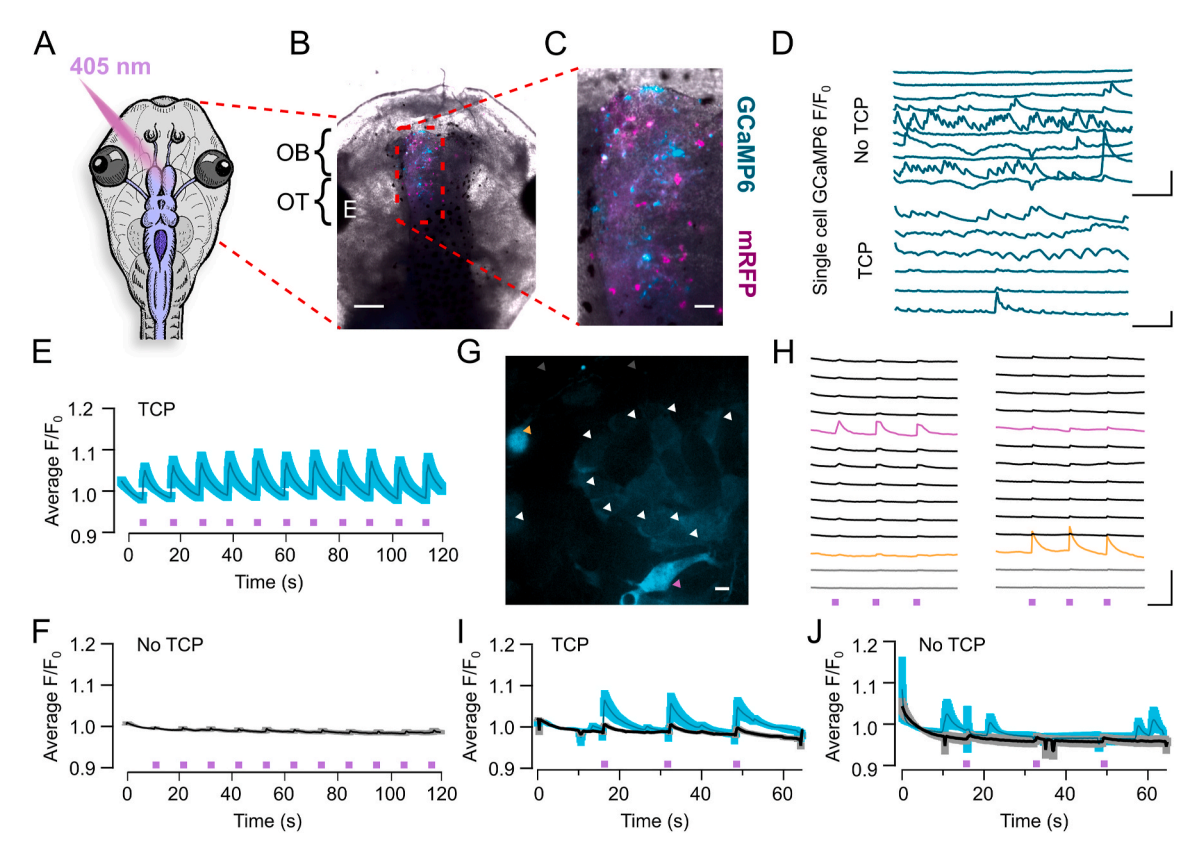


Fig. 6. In vivo photocontrol of single-neuron activity by TCP9 in Xenopus larvae. a) Schematic drawing of a Xenopus laevis tadpole head. b-c) Dorsal photographs of the tadpole brain through the translucent skin and skull showing the olfactory bulb (OB) and the optic tectum (OT). The letter "E" indicates an eye. OB neurons were electroporated with GCaMP6s and mRFP at developmental stage 28-30 and recorded at stage 42-45 (5-8 days later). Scale bars correspond to 100 µm (b) and 20 μm (c). d) Spontaneous calcium activity recorded in single cells in TCP-untreated (top) tadpoles or in TCP-treated (bottom) tadpoles (250 μM TCP9, 15 min, pH 7.6) without photostimulation. These neurons displayed high spontaneous activity compared to others that were relatively silent (e.g. see panel h). Scale bars represent 20 s, 0.1-fold (F/F₀) top, and 0.2-fold (F/F₀) bottom. e) Time course of averaged GCaMP6s fluorescence signals in individual cells (n = 29 cells, from 4 tadpoles) after sequentially repeated whole-field TCP9 photoactivation with 405 nm laser pulses (violet squares, 0.37 mW for 50 ms), f) Time course of averaged GCaMP6s fluorescence signals in individual cells (n = 15, from 3 TCP-untreated tadpoles) after sequentially repeated whole-field photostimulation with 405 nm laser pulses (violet squares, 0.37 mW for 50 ms). g) Basal GCaMP6s fluorescence of electroporated OB neurons. Neurons indicated by purple and orange arrowheads were stimulated separately while recording the activity of these and neighboring neurons (white arrowheads). The grey arrowhead points to a background region without transfected neurons, to record the light leaked from the stimulation laser by the dichroic mirror. Scale bar, 5 µm. h) Time course of calcium signal in individual cells shown in (g). Single-cell spot stimulation by TCP9 after 500 ms light pulses of 405 nm, 0.37 mW (violet squares) evoked cell-specific increased fluorescence responses. Orange, purple, grey, and black traces in (h) correspond to orange, purple, grey, and white arrowhead-pointed cells in (g), respectively. Scale bars represent 5 s, $0.5 \text{-fold } (F/F_0)$. i) Time course of averaged GCaMP6s signals in TCP9-single photoactivated cells (n = 20 cells from 7 tadpoles, cyan trace, mean \pm SEM), and neighboring non-stimulated cells (n = 103 cells from 7 tadpoles, black trace, mean \pm SEM). j) Time course of averaged GCaMP6s signals in single-photostimulated cells in TCP-untreaded tadpoles (n = 5 cells, from 3 tadpoles, cyan trace, mean ± SEM), and neighboring non-stimulated cells (n = 21 cells from 3 tadpoles, black trace, mean \pm SEM).

other optical methods such as optogenetics and diffusible photopharmacological compounds. Unlike optogenetics, TCPs do not require genetic modifications, allowing the study and control of native receptors without the need to overexpress exogenous proteins. This can bypass common overexpression side-effects such as altered physiological processes in small compartments, like dendritic spines, or immune responses. Using this chemical approach, the ability to selectively target specific cell types via transcriptional promoters is traded off by pharmacologically targeting particular receptor types. Other tethered photopharmacological molecules designed to attach to exogenously introduced cysteines [33,57-60] offer both genetic and pharmacological specificity but still require genetic engineering. TCPs, in contrast, use an electrophilic reactive group, such as NHS-ester, to covalently conjugate to nucleophilic side chains like lysines, commonly found in proteins. While this chemical reaction is relatively non-specific, it is targeted to the desired receptor —and even to an individual residue—by means of the glutamate ligand in an "affinity labeling" process [43,58,61,62]. In the present study, we found that TCP9 targets endogenous AMPARs and KARs but not NMDARs in dissociated neuronal cultures and in brain

slices (Figs. 1 and 3 and S1). Importantly, the lack of cell-type specificity is virtually circumvented by the spatial precision of light activation (with some limitations, such as that dendritic trees from other neurons can overlap the illuminated neuron, which can be avoided using soma-targeted optogenetics). Therefore, the widespread binding of TCP9 can be exploited as a way to broadly "label" different cell types, while the experimental precision is conferred by the laser activation.

When compared to caged compounds, another non-genetic photopharmacological approach, TCPs offer several competitive advantages. For example, TCP9, once tethered to the receptor, remains functional for hours after washout (Figs. 2 and 4), making it less invasive than diffusible photoswitches [63–65] or caged glutamate, which must be continuously perfused at millimolar concentration in the solution [66, 67]. Moreover, TCP9 can be reversibly photoswitched, whereas caged compounds are released irreversibly and subject to diffusion and saturation in the tissue [68–70]. As tethered ligands are conjugated near the glutamate binding site, they reach very high effective local concentration [58]. This, together with the thermal stability of *cis* active isomer [43], allows for robust responses with short illumination pulses and low

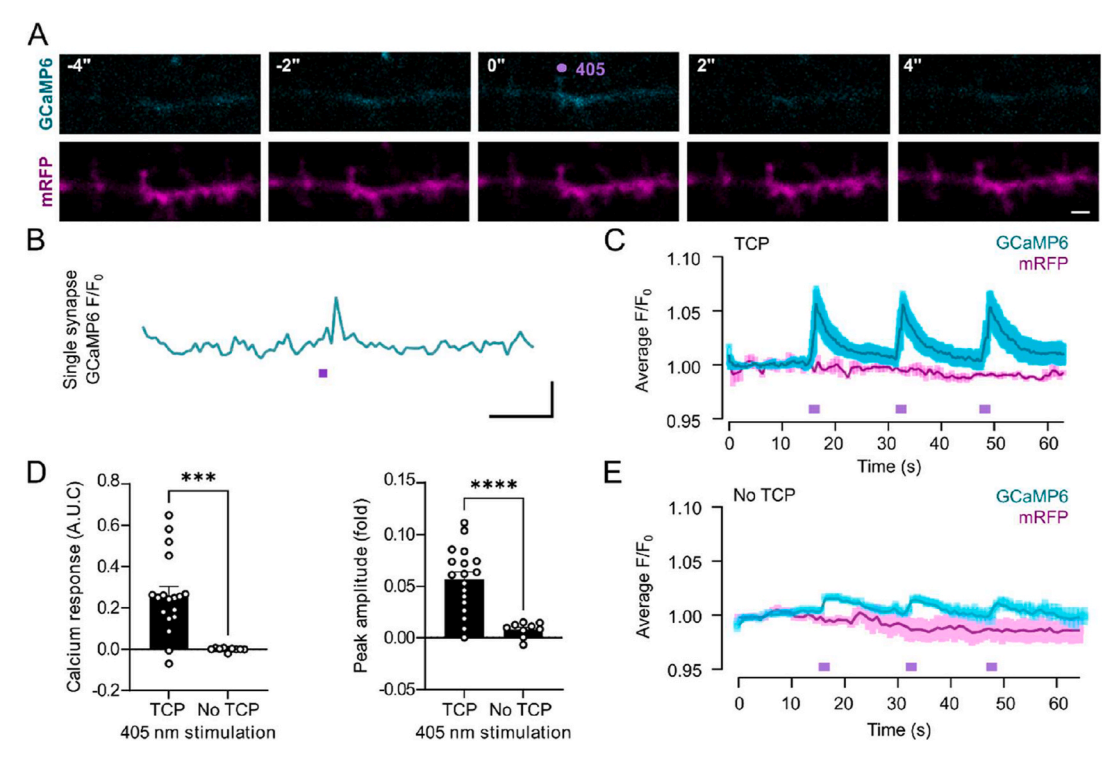


Fig. 7. TCP9 enables the photocontrol of single synapses *in vivo*. a) Time-lapse images of a spiny dendrite of a *Xenopus laevis* OB neuron electroporated with GCaMP6s (cyan) and mRFP (magenta) at developmental stage 28–30 and recorded 8 days later. Tadpoles were incubated once with 250 μM TCP9 for 15 min, and evoked activity experiments were carried out in the next 5 h. Scale bar 2 μm. b) Time course of GCaMP6s fluorescence signal from a single dendritic spine photostimulated by a 500 ms spotlight of 405 nm laser (0.37 mW, violet rectangle). Scale bars indicate 0.02 F/F₀ and 10 s. c) Time course of averaged GCaMP6s and mRFP fluorescence signals (mean \pm SEM) normalized to baseline (F/F₀) of consecutive photoactivations (405 nm, 500 ms, 0.37 mW, each violet rectangle) of n = 3 single dendritic spines from 3 different tadpoles *in vivo*. d) Comparison of overall photoresponses measured as area under the curve (AUC) of integrated GCaMP6s fluorescence signals and peak amplitude (fold of F/F₀) between TCP-treated tadpoles (data shown in panel c) and TCP-untreated tadpoles (data shown in panel e). Statistical analysis by Mann-Whitney test (***p = 0.0005) for AUC, and unpaired *t*-test with Welch's correction (****p < 0.0001) for peak amplitude. e) Time course average of GCaMP6s and mRFP fluorescence signals (mean \pm SEM) normalized to baseline (F/F₀) in single spines in OB cells in control TCP9-untreated tadpoles after 3 consecutive 500 ms photostimulations (405 nm, 0.78 mW, violet rectangles, n = 3 different spines from the same tadpole).

light power, which reduces the risk of phototoxicity. Indeed, we observed that TCP9-conjugated neurons in *ex vivo* and *in vivo* neuronal ensembles (Figs. 2, 5 and 6) show spontaneous activity, suggesting that the treatment causes little or no perturbation prior to photostimulation. Although caged glutamate compounds are very useful in brain slices [70, 71], they can inhibit endogenous GABAAR at the concentrations required for uncaging [69,72] and are challenging to use *in vivo* due to the need to perfuse them continuously in the brain to achieve repeatable photoresponses [72–74]. In this line, high molecular weight cages have been recently developed to tackle these constraints [75].

We leveraged the unique properties of TCP9 to overcome several limitations of photostimulation in neurobiology, notably the control of endogenous receptors at single synapses in vivo. With this aim, we thoroughly tested TCP9 across experimental preparations of increasing technical complexity and physiological relevance: from twodimensional cultures of dissociated neurons in vitro (Fig. 1), to threedimensional organotypic brain slices ex vivo (Figs. 2-5), and to intact brains of whole organisms in vivo (Figs. 6-7). We utilized multiple optical techniques: from whole-field illumination with a monochromator (Fig. 1, S1-S3) to both whole-field (Figs. 2-4, and 6) and single-spot scanning with a laser beam (Figs. 5 and 7). We also covered different neuronal activity readouts: patch clamp electrophysiology (Fig. 1) and calcium fluorescence imaging with chemical (Fig. S7) and genetically encoded sensors (Figs. 2-7). By combining all these approaches, we successfully explored the spatiotemporal limits of TCP9 and demonstrated efficient control of neuronal and synaptic activity at several scales: photoactivation of (1) neuronal ensembles simultaneously (Figs. 1-4, and 6), of (2) individual neurons independently (Figs. 5 and

6), and of (3) single synapses *ex vivo* and *in vivo* (Figs. 5 and 7), the latter being at the spatial resolution limit of conventional optical microscopy.

In our experiments involving the photocontrol of multiple neurons within neuronal ensembles in complex tissue (ex vivo and in vivo) we estimate that about half of the cells were responsive upon TCP9 incubation, and from these, almost all (~90 %) could be reversibly photocontrolled. After the treatment, cells did not display irreversible increases in intracellular calcium levels or loss of neuronal morphology that can be associated with toxicity or death. In our hippocampal samples, we observed TCP9-photoresponding cells of diverse morphologies, compatible with pyramidal, stellate, excitatory, inhibitory neurons, and possibly glial cells. They could be found as deep as 145 µm in organotypic brain slices (Fig. S4) and \sim 60 µm in the intact brain of tadpoles, demonstrating that TCP9 can penetrate deep into neuronal tissue presumably through intercellular spaces, as the charged TCP9 ligand is membrane impermeant. Importantly, photoresponses were stably sustained over long periods of time. A single TCP9 incubation resulted in labeled GluRs that quantitatively maintained their functional photoresponses for over 4 h (Fig. 4) and up to 8 h (Fig. 2h) with no signs of photobleaching or photo-fatigue. This suggests that neither TCP9 conjugation nor photoactivation events (lasting a few seconds or minutes) impair GluR functionality or cellular dynamics per se, which offers a wide experimental window for long-term studies of receptor activity, localization and dynamics, as well as studies of connectivity between neurons in genetically unaltered circuits.

The capabilities of TCP9 were put to the test in two novel applications: 1) the photocontrol of single synapse activity, and 2) the study of endogenous GluR dynamics during events of synaptic plasticity. The first

one was achieved under nearly physiological conditions, such as the rat organotypic slices (Fig. 5), and in the intact brain of live tadpoles (Fig. 7). These achievements push the spatiotemporal boundaries of photoactivation to the limit, given that the typical spine size and the resolution of optical microscopes is $\sim\!1~\mu m$ and the action potential kinetics is $\sim\!1$ ms. Neuronal firing rate could be photocontrolled at 1–10 Hz using TCP9 (Fig. 1), equivalent to what is typically reported using caged glutamate [76]. Other PTLs have also been reported to activate single synapses but still require genetic manipulation [57]. Thus, the performance of TCP9 is comparable to that of caged glutamate [77], with added advantages like photoreversibility, preference for AMPAR/KARs, and long-lasting use without the need of continuous perfusion, making it particularly suited for *in vivo* applications.

Note that photocontrolling single synapses with optogenetics is challenging, due in part to the low chord conductance and calcium permeability of channelrhodopsins compared to that of postsynaptic GluRs and the resulting need to overexpress a large copy number in a constrained subcellular compartment [78–80]. Overall, robust tools to photocontrol and read out the activity of single synapses with pharmacological precision are required to determine experimentally the complex transfer function of dendrites [81,82].

Regarding the application of TCP9 to study native receptor dynamics, we chose a well-known phenomenon of synaptic plasticity – the internalization of AMPARs during NMDAR-dependent LTD [83]. TCP9 offers an unprecedented opportunity to monitor the presence of functional photoresponsive receptors at the neuronal membrane, by recording the responses to fixed photostimuli. Prior to LTD induction, we efficiently tracked the calcium responses of functional TCP9-labeled AMPAR/KARs, which were stable for 2 h. Upon LTD induction, those responses were reduced by ~25 % for about 2 more hours (Fig. 4), consistent with the internalization of AMPARs into cytoplasmatic recycling vesicles as reported during NMDAR-LTD [48,49]. Once removed from the plasma membrane, TCP9-labeled receptors no longer contribute to the calcium signal regardless of their (photo)activation state. Thus, TCP9 allows not only monitoring the dynamics of endogenous AMPAR/KARs but also quantifying the receptors that are functional on the cell membrane. The use of calcium imaging as functional readout, however, bears some limitations. As it is an indirect and non-linear method to detect receptor activity, it may not directly reflect changes in receptor number or localization. Moreover, although TCP has the potential to label any type of AMPAR and KAR, calcium imaging is limited to tracking calcium-permeable receptors or receptors functionally coupled to calcium channels. Based on the GluR subunit expression in the rat hippocampus at the developmental stage used in our experiments [84-88], we believe the calcium responses that we observe are most likely mediated by GluK1 (as demonstrated in Ref. [43]) and/or GluA1 subunits. Other calcium-mobilizing mechanisms activated by TCP9-conjugated receptors (e.g. via the endoplasmic reticulum) could also be possible. Another limitation, intrinsic to many labeling methods, is that TCP9 can track removal but not incorporation of new receptors into the plasma membrane, as internal receptors are not conjugated during the initial incubation. Anyway, compared to other molecular, electrophysiological, and optical techniques to study GluR dynamics, only TCPs combine the longitudinal and real-time tracking of endogenous receptors with the ability to detect and control their function. Classical biochemical tools such as biotin and radioisotopes were the first ones to allow quantifying endogenous receptors, but they offer a static off-line view, rather than a longitudinal real-time view. Fluorescent tools, such as fluorescent proteins, photoactivatable proteins, super ecliptic pHluorin, etc., allow real-time longitudinal tracking of receptors but require genetic manipulation and/or overexpression of exogenous GluRs. There are many alternative methods to label receptors such as SNAP-tag, Halotag, small immunoreactive tags, and photoswitchable tethered ligands (PTLs and PORTLs) [7,30,89]. All of them, however, suffer from the same limitation - the need for genetic engineering. Recently developed techniques permit the labeling of endogenous GluRs

using ligand-directed chemical methods [28,29] but they cannot detect whether the receptors are functional nor allow controlling their activity.

The fact that TCP9-conjugated receptors can be detected for at least 8 h is consistent with the reported lifetime of AMPARs (from synthesis to proteolysis), which is between 33 h [28] and 48 h [10,11]. The presence of photoresponses also demonstrates that TCP9-conjugated receptors are not targeted for degradation - instead, they are most likely recycled between the synaptic and extrasynaptic regions [90,91] on a timescale of seconds (although we cannot distinguish these populations by photoswitching TCP9), and between cell membrane and internal recycling vesicles on a timescale of minutes (which we can detect with TCP9 because they stop producing photoresponses once internalized). We could eventually distinguish between the synaptic and the extrasynaptic pools of GluRs because the latter one would respond to TCP9 photostimulation but not to presynaptically released glutamate, while the synaptic pool would respond to both stimuli. Overall, we envisage great potential for TCP9 in pulse-and-chase experiments aimed at studying functional receptor dynamics during endocytosis and exocytosis, as well as other events of neuronal plasticity, such as recycling dynamics in early and late phases of LTP and LTD, homeostatic plasticity, neuronal oscillations, and circuit connectivity. This potential applies to in vitro, ex vivo, and most needfully, in vivo preparations.

One of the most promising applications of TCP9 is, precisely, its use in vivo in genetically unaltered organisms. TCPs have already been employed as proof-of-concept molecular prostheses to restore visual responses [43] and auditory responses with light [44]. Here, we used wild-type Xenopus tadpoles as a convenient model to carry out all-optical experiments in vivo. Tadpoles have translucent skulls and skin that facilitate photostimulation and fluorescence imaging. They are amenable to electroporation of exogenous genes like fluorescent sensors and optogenetic actuators, as well as to photopharmacological interventions. Remarkably, unlike other small animals, Xenopus feature spiny neurons [54], which allows spine (patho)physiology to be studied in an alternative model to reduce or replace the use of higher vertebrates like rodents in neurobiology, adhering to ethical principles [92]. Xenopus larvae have already been used in immunology [93,94], microbiology [95], cancer [96], toxicology [97], and drug screening studies [98], and serve as excellent models to study axonal growth and development [99,100]. For example, we are currently using TCPs to photoactivate endogenous receptors in specific cells at specific times to explore the role of receptor activity in the development of axons and dendrites.

The existing TCP technology can be further improved in several ways for basic research in neurophysiology and for therapeutical applications. First, the violet light required to photoactivate GluRs has limited tissue penetration and can damage cells, compared to longer wavelengths. Red-shifting the TCP excitation wavelength has been achieved using push-pull mechanisms [44,101] and tetra-*ortho*-chloro substitutions, as done in cysteine-targeted PTLs [102]. Another promising option for basic research involves using two- and three-photon excitation with near- and mid-infrared pulsed lasers, which not only offer millimeter-range tissue penetration but also enable micrometer-scale focused activation in three dimensions [46,47,103–106]. Additionally, the chemical preparation and use of TCP9 could benefit from faster and more selective click reagents that do not require a copper catalyst, as well as faster protein-reactive groups that would reduce the TCP incubation time and concentration in tissue.

In conclusion, we have comprehensively evaluated the capabilities of TCP9 to photocontrol neuronal activity across multiple spatiotemporal scales. Our findings demonstrate that this molecule is an outstanding photopharmacological tool to manipulate the function of GluRs at single synapses *ex vivo* and *in vivo*. It enables the study of endogenous GluR physiology and the control of neuronal and synaptic activity in an efficient, long-lasting, reversible, and minimally invasive way, without the need for genetic engineering.

4. Methods

Preparation of TCP9 by click reaction. TCP9 was generated prior to attachment to the target protein by fusing two components via a copper(I)-catalyzed azide—alkyne cycloaddition reaction (click chemistry). The first component containing the azide group ("head" group) bears the glutamate and the azobenzene moieties. This component reacts with the second component containing the alkyne group ("tail" group), which bears the NHS ester anchoring moiety [43,44]. A solution in water of the "head" group (1 equiv), Cu_2O (2.4 equiv), and ascorbic acid (4 equiv) was stirred for 5 min at room temperature (r.t.) in a 1.5 mL Eppendorf tube. To this mixture, a solution of the "tail" group (1.1 equiv) in tetrahydrofuran (THF) was added and vortexed for 30 min at r. t. This final mixture was diluted 10 times in dimethylsulfoxide (DMSO), vortexed, and centrifuged for 1 min to separate the insoluble Cu_2O particles. TCP9 stock solution at 12 mM was aliquoted to be used immediately or stored at $-20\,^{\circ}\text{C}$.

Hippocampal neuronal primary cultures. All procedures involving animals were conducted in accordance with the European guidelines for animal care and use in research and were approved by the Animal Experimentation Ethics Committee at the University of Barcelona (Spain). Low-density primary hippocampal cultures were prepared from postnatal day (P) P0-P3 Sprague Dawley rat pups and maintained for 1–2 weeks in coverslips coated with poly-L-lysine (Sigma-Aldrich), as previously described [107]. Cells were cultured with complete medium (Neurobasal A, 2 % B-27, 0.5x GlutaMax, 15 mM glucose, 5 U/ml penicillin, and 5 μ g/ml streptomycin). Anti-mitotic treatment with 5 μ M AraC was applied after 48–72 h to avoid fibroblast and astrocyte proliferation. The culture medium was refreshed every 3–4 days by replacing half of the volume.

Electrophysiological recordings. Voltage and current-clamp recordings under whole-cell configuration were performed using an EPC-10 amplifier, and data was acquired at 10 kHz through Patch Master (HEKA) software. Bath solution was composed of 140 mM NaCl, 1 MgCl₂, 2.5 mM KCl, 10 mM HEPES, 2.5 mM CaCl₂ and 10–20 mM glucose (to adjust osmolarity to 310 mOsm/kg), pH 7.42 adjusted with NaOH. Borosilicate glass pipettes were pulled with a typical resistance of 6–8 MΩ and filled with a solution containing 130 mM KCl, 5 mM MgCl₂, 3 mM Na₂ATP, 1 mM Na₂GTP, 20 mM HEPES, 0.5 mM EGTA, pH 7.2 adjusted with KOH, and osmolarity adjusted at 289 mOsm/kg. During recordings, neurons were maintained at r.t. (25–27 °C) in a continuous perfusion of bath solution.

TCP9 conjugation and photostimulation in neuronal primary cultures. Prior to recording, neurons were incubated with TCP9 (12-25 μM) for 2 min, at r.t., in the absence of light, in a bath solution composed of 100 mM NaCl, 1 mM MgCl₂, 2.5 mM KCl, 2.5 mM CaCl₂, 10 mM glucose, and 2.7 mM Na₂CO₃, 47.3 mM NaHCO₃, 310 mOsm/kg, pH 9 adjusted with NaOH. Before placing the coverslip in the recording chamber, cells were washed again with fresh bath solution. Light stimulation was done by illumination of the entire focused field using a Polychrome V monochromator (TILL Photonics) connected through the back port of an IX71 inverted microscope (Olympus) with a CP-ACHROMAT 40x/0.65 objective (Zeiss). Wavelengths were automatically controlled by connecting the monochromator to the EPC-10 amplifier via Photochromic Manual Control (TILL Photonics) and using the photometry module of Patch Master. Light power density measured with a Newport 1916-C light-meter after the objective was: 1.6 mW mm⁻² for 425 nm, 0.8 mW mm⁻² for 380 nm, and 1.8 mW mm^{-2} for 500 nm.

Organotypic hippocampal slice cultures and gene transfection. Hippocampal organotypic slice cultures were prepared from P6-8 rats as described [71,108]. Slices of 400 μm of thickness were cultured at 35 $^{\circ} C$ on interface membranes (Millipore) and fed with MEM media containing 20 % horse serum, 27 mM D-glucose, 6 mM NaHCO3, 2 mM CaCl2, 2 mM MgSO4, 30 mM HEPES, 0.01 % ascorbic acid and 1 $\mu g/ml$ insulin. pH was adjusted to 7.3 and osmolality to 300–320 mOsm/kg. Slices were

biolistically transfected (BioRad) after 5–7 days *in vitro* (DIV) with plasmids expressing GCaMP6s (Addgene) under the CMV promoter, and DsRed2 under the CAG promoter, as described [71,108].

TCP9 conjugation in organotypic slice cultures. Hippocampal slice cultures were incubated in 250 μ M TCP9 for 15 min at r.t. in darkness in modified artificial cerebrospinal fluid (ACSF: 119 mM NaCl, 2.5 mM KCl, 3 mM CaCl₂, 0.2 mM MgCl₂, 26.2 mM NaHCO₃, 1 mM NaH₂PO₄ and 11 mM glucose, pH 7.4), equilibrated with carbogen (5 % CO₂/95 % O₂). After 3 washouts (lasting 1, 5, and 5 min), slices were placed on the microscope recording chamber.

Photostimulation and calcium imaging in organotypic slices. Time-lapse fluorescence imaging was carried out in the Advanced Digital Microscopy Core Facility of IRB (Barcelona Research Institute) using a SP5 spectral confocal multiphoton microscope (Leica) equipped with a 405 nm CW diode laser, and an Argon laser (488 and 514 nm). We used a 40x/1.25-0.75-NA Oil objective (HCX PL APO, Leica). Imaging was performed at 8-15 DIV. After TCP9 conjugation, hippocampal slices were maintained in the microscope recording chamber at r.t. in a continuous perfusion (at 2–3 ml/min) of carbogenated ACSF. Slices with pyramidal neurons co-expressing GCaMP6s and DsRed2, healthy morphology and no signs of fluorescent aggregates were selected. In whole-field imaging experiments, green and red fluorescent proteins were simultaneously excited at 488 nm using a bidirectional laser scanning at 400 Hz in a single focused plane. Images were recorded with a resolution of 512 \times 512, at 343 ms per image, with an imaging interval of 4 s. Green fluorescence emission was detected in the 500-550 nm range, and red fluorescence in the 569-648 nm range. Pinhole aperture was set at maximum (600 µm). Whole-field TCP photostimulation was carried out in periods of 1 min of sequential illumination with the 405 nm (0.81 mW μm^{-2}) and the 514 nm (0.35 mW μm^{-2}) lasers at 256 \times 256 resolution with bidirectional laser scan, intermixed between image acquisition to keep the 4 s imaging interval. In single-cell stimulation experiments, photostimulation was performed by scanning a region of interest (ROI) containing the soma of the neuron with the 405 nm laser for 10-20 s, intermixed with the image acquisition every 2 s. Since the 488 nm laser is more focused and intense in these experiments, the green light is not required to switch off TCP9. In single-spine experiments, imaging was similarly performed, using a 63x/1.4-NA Oil Lbd BL objective (HCX PL APO, Leica) and higher digital zoom, and photostimulation was performed with 1 s flashes of the 405 nm laser focused in one spotlight close to the tip of the spine (0.25 mW μ m⁻²), using the Flymode FRAP module of the SP5 Leica software. At the end of each experiment, we confirmed that the neuron kept its healthy morphology.

Xenopus laevis embryo maintenance. *Xenopus laevis* embryos obtained from *in vitro* fertilization were raised in 0.1X Modified Barth's saline (MBS; 8.8 mM NaCl, 0.1 mM KCl, 82 μM MgSO₄, 0.24 mM NaHCO₃, 0.1 mM HEPES, 33 μM Ca(NO₃)₂, 41 μM CaCl₂, pH 7.6) at 14–22 °C, and staged according to the table of Nieuwkoop and Faber [109]. This research has been regulated under the Animals (Scientific Procedures) Act 1986 Amendment Regulations 2012 following ethical review by the University of Cambridge Animal Welfare and Ethical Review Body (AWERB).

Electroporation of *Xenopus* embryos. Olfactory bulb electroporation procedure was modified from [55,56]. Stage 28 embryos were anaesthetized in 0.4 mg/ml MS222 in 1X MBS. The central ventricle between olfactory bulbs was injected with the electroporation mixture (1 μ g/ μ l of GCaMP6s:mRFP; 2:1), followed by 8 squared electric pulses of 50 ms duration at 1000 ms intervals, delivered at 18 V. The embryos were recovered and raised in 0.1X MBS until the desired embryonic stage.

TCP9 conjugation in *Xenopus* embryos. Around 5–8 days after electroporation, embryos were anaesthetized with 0.4 mg/ml MS222 in 1X MBS. The surface of the tadpole brain was exposed by removal of the overlying epidermis. The tadpole was incubated in 250 μM TCP in 1X MBS, pH 7.6, for 15 min at r.t. and washed out 2 times, before the imaging session.

In vivo photostimulation and calcium imaging. *Xenopus* embryos were mounted in an oxygenated chamber created with Permanox slides (Sigma-Aldrich) and Gene Frame (ThermoFisher) and bathed in 1X MBS with 0.1 mg/ml MS222. Detection of the electroporated OB cells was performed with a Plan Fluor 20X (NA 0.5) objective in a Nikon Eclipse TE2000-U inverted microscope equipped with an EM-CCD camera (Hamamatsu Image Flash 4.0V2 C11440). Real-time calcium imaging was performed using a 60X UPLSAPO objective (NA 1.3) in a PerkinElmer Spinning Disk UltraVIEW ERS, Olympus IX81 inverted spinning disk confocal microscope. Z-stack images (1-2 µm apart) were acquired with Volocity (PerkinElmer) at a resolution of 1024×1024 , with 561nm laser (Cobolt Jive) for excitation of mRFP in combination with a 600/37 emission filter (Semrock). Exposure time and 561 nm laser power (0.95–2 mW) were set to obtain the optimal signal-to-noise ratio (SNR). GCaMP6s was excited with 488 nm-laser (Coherent Sapphire) in combination with a 525/45 emission filter (Semrock). Exposure time was set to 200 ms and laser power was adjusted to the optimal SNR (0.9-1.72 mW). GCaMP6s and mRFP fluorescence were acquired using the same dichroic beam splitter (Chroma ZT405/488/561/640rpc). Both laser beams were circularly polarized via a quarter wave plate (Thorlabs AOWP05) to excite fluorescent proteins homogeneously regardless of their orientation.

Whole-field photostimulation of TCP9 was performed by scanning the 405 nm laser at 1024×1024 resolution for 50 ms (1.29 mW). Single-cell photostimulation was performed by spotlight on the cell soma for 500 ms (0.37 mW) and single-spine photostimulation by flashing the 405 nm laser at one spotlight next to the tip of the spine for 500 ms (0.37 mW). The parameters for spotlight activation of TCP9 were set in the PhotoKinesis control Unit for FRAP as: 2" for PK cycles; "1" for PK step size; "500 ms' for PK spot period; "30" for PK spot cycles; "Small' for PK spot size; "None' for PK attenuation. Images for GCaMP6s and mRFP were captured immediately before and after FRAP photostimulation for 15 s intervals pre- and post-photostimulation. Exposure time (139–800 ms) and laser power (0.9–1.72 mW) were adjusted to the optimal SNR.

Data analysis and statistics. Amplitude of photocurrents was analyzed using IgorPro (Wavemetrics), Microsoft Excel (Microsoft), and Origin. Time-lapse images from organotypic slices and in vivo Xenopus experiments were analyzed using Fiji/ImageJ [110]. A ROI was outlined around the soma of each cell and the total fluorescence values for the green and the red channels were measured at each time point. In the case of single-spine experiments, the ROI was outlined around the dendritic spine, including half of the neck. Fluorescence values (F) were normalized with respect to baseline by dividing each time point by the average of all values before any stimulation (F₀). "Average F/F₀" values were obtained by averaging normalized values of each cell (or spine) from different slices. All values are expressed as mean \pm SEM (standard error of the mean). Cells were considered photoresponsive if at least one time point of the GCaMP6s fluorescence signal in the soma increased >50 % over baseline after violet illumination. The area under the curve (AUC) of the integrated GCaMP6 fluorescence intensity signal was measured from the onset of the violet illumination until the end of the green illumination, in whole-field stimulation experiments. AUC was measured during the first 2 min after violet light onset in single-cell experiments, and during the first 15 s after violet light pulse in single-spine experiments. Statistical significance was set at the 95 % confidence level (two tailed) and calculated using GraphPad Prism. Normality was analyzed using Shapiro-Wilk test. Kruskal-Wallis test with Dunn's multiple comparison test was used to compare the pharmacological groups with respect to vehicle in Fig. 3. Student's paired t-test was used to calculate differences in amplitude photoresponses between the last 60 min period (85'-125') and the 60 min baseline period before LTD induction in Fig. 4. In Fig. 7, calcium response AUC was analyzed by Mann-Whitney test, and peak amplitude by unpaired t-test with Welch's correction. In supplementary figures, spike probability and amplitude was analyzed by Mann-Whitney test (Fig. S1); photocurrent amplitudes by paired t-test (Fig. S2); ex vivo single cells and single spines

parameters by ANOVA with Tukey's multiple comparison test and Kruskal-Wallis test with Dunn's multiple comparison (Fig. S5); *ex vivo* glutamate comparison by Mann-Whitney test (Fig. S8).

In Fig. 3, pharmacological treatments and vehicle experiments were performed in an interleaved way, each one in a different slice but within the same experimental day. Similarly, we did control experiments without TCP conjugation but with the same duration and intensity of photostimulation in an interleaved way with those with TCP conjugation. The order of control and experimental conditions were randomly swapped.

CRediT authorship contribution statement

Aida Garrido-Charles: Writing - review & editing, Writing - original draft, Visualization, Methodology, Investigation, Formal analysis, Data curation, Conceptualization. Miquel Bosch: Writing – review & editing, Writing - original draft, Visualization, Supervision, Methodology, Investigation, Funding acquisition, Formal analysis, Data curation, Conceptualization. Hyojung Lee: Investigation, Formal analysis. Xavier Rovira: Investigation. Silvia Pittolo: Investigation. Artur Llobet: Supervision, Resources, Methodology. Hovy Ho-Wai Wong: Writing review & editing, Supervision, Methodology. Ana Trapero: Resources. Carlo Matera: Visualization, Supervision, Resources. Claudio Papotto: Investigation. Carme Serra: Resources, Funding acquisition. Amadeu Llebaria: Supervision, Funding acquisition. Eduardo Soriano: Supervision, Resources. Maria V. Sanchez-Vives: Supervision, Funding acquisition. Christine E. Holt: Supervision, Funding acquisition. Pau Gorostiza: Writing - review & editing, Writing - original draft, Supervision, Project administration, Funding acquisition, Conceptualization.

Declaration of competing interest

The authors declare that they have no known competing financial interests or personal relationships that could have appeared to influence the work reported in this paper.

Acknowledgements

We are grateful to Bernardo Sabatini, Rob Malenka, Richard Huganir, Katherine Roche, and Arnaud Gautier for useful discussions; to Núria Camarero, Antoni Parcerisas, Ashraf Muhaisen, Beatrice Terni, Francisco Ciruela, Anna Lladó, and Lídia Bardia for advice, help and support, and to Carlos Aizenman and Arseny Khakhalin for inspiring the Xenopus drawing. This research received funding from the European Union Research and Innovation Programme Horizon 2020 - Human Brain Project SG3 (945539), DEEPER (ICT-36-2020-101016787), European Innovation Council Pathfinder Open (PHOTOTHERAPORT, 101130883), Agency for Management of University and Research Grants/Generalitat de Catalunya (CERCA Programme; 2021-SGR-01410 and AGAUR 2021-SGR-01165), Fonds Européen de Développement Économique et Régional (FEDER) funds, Ministry of Science and Innovation grants PID2019-111493RB-I00 (DEEP RED), PID2022-142609OB-I00 (EPILLUM), PID2020-118817GB-I00 (SynWAVE) and PID2023-152918OB-I00 (INFRASLOW), Fundaluce and "la Caixa" foundations (ID 100010434, agreement LCF/PR/HR19/52160010). A. G.-C. was supported by a predoctoral fellowship FPI (BES-2014-068169) and an Alexander von Humboldt postdoctoral fellowship. M.B. was supported by a Marie Sklodowska-Curie Reintegration Grant (H2020-MSCA-IF-2014).

Appendix A. Supplementary data

Supplementary data to this article can be found online at https://doi.org/10.1016/j.brs.2025.09.005.

References

- Gereau RWI, Swanson GT, editors. The glutamate receptors. Totowa, NJ: Humana Press: 2008
- [2] Traynelis SF, Wollmuth LP, Mcbain CJ, Menniti FS, Vance KM, Ogden KK, Dingledine R. Glutamate receptor ion channels: structure, regulation, and function. Pharmacol Rev 2010;62(3):405–96. https://doi.org/10.1124/ pr.109.002451.405.
- [3] Luscher C, Malenka RC. NMDA receptor-dependent long-term potentiation and long-term depression (LTP/LTD). Cold Spring Harbor Perspect Biol 2012;4(6): a005710. https://doi.org/10.1101/cshperspect.a005710. a005710.
- [4] Choquet D, Triller A. The dynamic synapse. Neuron 2013;80(3):691–703. https://doi.org/10.1016/j.neuron.2013.10.013.
- [5] Groc L, Choquet D. Linking glutamate receptor movements and synapse function. Science (New York, NY) 2020;368(6496). https://doi.org/10.1126/science. aay4631.
- [6] Malinow R, Malenka RC. AMPA receptor trafficking and synaptic plasticity. Annu Rev Neurosci 2002;25:103–26. https://doi.org/10.1146/annurev. neuro.25.112701.142758.
- [7] Restituito S, Ziff EB. In: Kittler JT, Moss SJ, editors. Methods for uncovering the mechanisms of AMPA receptor trafficking; 2006. Boca Raton (FL).
- [8] Chen I, Howarth M, Lin W, Ting AY. Site-specific labeling of cell surface proteins with biophysical probes using biotin ligase. Nat Methods 2005;2(2):99–104. https://doi.org/10.1038/nmeth735.
- [9] Ehlers MD. Reinsertion or degradation of AMPA receptors determined by activity-dependent endocytic sorting. Neuron 2000;28(2):511–25. https://doi.org/ 10.1016/S0896-6273(00)00129-X
- [10] Archibald K, Perry MJ, Molnár E, Henley JM. Surface expression and metabolic half-life of AMPA receptors in cultured rat cerebellar granule cells. Neuropharmacology 1998;37(10–11):1345–53. https://doi.org/10.1016/s0028-3908(98)00135-x.
- [11] Cohen LD, Zuchman R, Sorokina O, Müller A, Dieterich DC, Armstrong JD, Ziv NE. Metabolic turnover of synaptic proteins: kinetics, interdependencies and implications for synaptic maintenance. PLoS One 2013;8(5):e63191. https://doi. org/10.1371/journal.pone.0063191.
- [12] O'Brien RJ, Kamboj S, Ehlers MD, Rosen KR, Fischbach GD, Huganir RL. Activity-dependent modulation of synaptic AMPA receptor accumulation. Neuron 1998;21 (5):1067–78. https://doi.org/10.1016/s0896-6273(00)80624-8.
- [13] Shi SH, Hayashi Y, Petralia RS, Zaman SH, Wenthold RJ, Svoboda K, Malinow R. Rapid spine delivery and redistribution of AMPA receptors after synaptic NMDA receptor activation. Science (New York, NY) 1999;284(5421):1811–6. https:// doi.org/10.1126/science.284.5421.1811.
- [14] Ashby MC, De La Rue SA, Ralph GS, Uney J, Collingridge GL, Henley JM. Removal of AMPA receptors (AMPARs) from synapses is preceded by transient endocytosis of extrasynaptic AMPARs. J Neurosci: Off J Soc Neurosci 2004;24 (22):5172–6. https://doi.org/10.1523/JNEUROSCI.1042-04.2004.
- [15] Kopec CD, Li B, Wei W, Boehm J, Malinow R. Glutamate receptor exocytosis and spine enlargement during chemically induced long-term potentiation. J Neurosci: Off J Soc Neurosci 2006;26(7):2000–9. https://doi.org/10.1523/ JNEUROSCI.3918-05.2006.
- [16] Tatavarty V, Sun Q, Turrigiano GG. How to scale down postsynaptic strength. J Neurosci: Off J Soc Neurosci 2013;33(32):13179–89. https://doi.org/10.1523/ JNEUROSCI.1676-13.2013.
- [17] Keppler A, Gendreizig S, Gronemeyer T, Pick H, Vogel H, Johnsson K. A general method for the covalent labeling of fusion proteins with small molecules in vivo. Nat Biotechnol 2003;21. https://doi.org/10.1038/nbt765. United States.
- [18] Los GV, Encell LP, McDougall MG, Hartzell DD, Karassina N, Zimprich C, Wood KV. HaloTag: a novel protein labeling technology for cell imaging and protein analysis. ACS Chem Biol 2008;3(6):373–82. https://doi.org/10.1021/ ch800025k
- [19] Lissin DV, Gomperts SN, Carroll RC, Christine CW, Kalman D, Kitamura M, von Zastrow M. Activity differentially regulates the surface expression of synaptic AMPA and NMDA glutamate receptors. Proc Natl Acad Sci USA 1998;95(12): 7097–102. https://doi.org/10.1073/pnas.95.12.7097.
- [20] Dieterich DC, Hodas JJL, Gouzer G, Shadrin IY, Ngo JT, Triller A, Schuman EM. In situ visualization and dynamics of newly synthesized proteins in rat hippocampal neurons. Nat Neurosci 2010;13(7):897–905. https://doi.org/10.1038/nn.2580.
- [21] Tsai Y-H, Essig S, James JR, Lang K, Chin JW. Selective, rapid and optically switchable regulation of protein function in live mammalian cells. Nat Chem 2015;7(7):554–61. https://doi.org/10.1038/nchem.2253.
- [22] Hayashi Y, Shi SH, Esteban JA, Piccini A, Poncer JC, Malinow R. Driving AMPA receptors into synapses by LTP and CaMKII: requirement for GluR1 and PDZ domain interaction. Science (New York, NY) 2000;287(5461):2262–7. https:// doi.org/10.1126/science.287.5461.2262.
- [23] Groc L, Lafourcade M, Heine M, Renner M, Racine V, Sibarita JB, Cognet L. Surface trafficking of neurotransmitter receptor: comparison between single-molecule/quantum dot strategies. J Neurosci 2007;27(46):12433–7. https://doi.org/10.1523/JNEUROSCI.3349-07.2007.
- [24] Mikuni T, Nishiyama J, Sun Y, Kamasawa N, Yasuda R. High-throughput, high-resolution mapping of protein localization in mammalian brain by in vivo genome editing. Cell 2016;165(7):1803–17. https://doi.org/10.1016/j.cell.2016.04.044.
- [25] Getz AM, Ducros M, Breillat C, Lampin-Saint-Amaux A, Daburon S, François U, Choquet D. High-resolution imaging and manipulation of endogenous AMPA receptor surface mobility during synaptic plasticity and learning. Sci Adv 2022;8 (30):eabm5298. https://doi.org/10.1126/sciadv.abm5298.

- [26] Graves AR, Roth RH, Tan HL, Zhu Q, Bygrave AM, Lopez-Ortega E, Huganir RL. Visualizing synaptic plasticity in vivo by large-scale imaging of endogenous AMPA receptors. eLife 2021;10. https://doi.org/10.7554/eLife.66809.
- [27] Kareemo DJ, Winborn CS, Olah SS, Miller CN, Kim JM, Kadgien CA, Kennedy MJ. Genetically encoded intrabody probes for labeling and manipulating AMPA-type glutamate receptors. Nat Commun 2024;15(1). https://doi.org/10.1038/s41467-024-54530-5
- [28] Ojima K, Shiraiwa K, Soga K, Doura T, Takato M, Komatsu K, Kiyonaka S. Ligand-directed two-step labeling to quantify neuronal glutamate receptor trafficking. Nat Commun 2021;12(1):831. https://doi.org/10.1038/s41467-021-21082-x.
- [29] Wakayama S, Kiyonaka S, Arai I, Kakegawa W, Matsuda S, Ibata K, Hamachi I. Chemical labelling for visualizing native AMPA receptors in live neurons. Nat Commun 2017;8. https://doi.org/10.1038/ncomms14850.
- [30] Rost BR, Schneider-Warme F, Schmitz D, Hegemann P. Optogenetic tools for subcellular applications in neuroscience. Neuron 2017;96(3):572–603. https:// doi.org/10.1016/j.neuron.2017.09.047.
- [31] Jerca FA, Jerca VV, Hoogenboom R. Advances and opportunities in the exciting world of azobenzenes. Nat Rev Chem 2022;6(1):51–69. https://doi.org/10.1038/ s41570-021-00334-w.
- [32] Kienzler MA, Isacoff EY. Precise modulation of neuronal activity with synthetic photoswitchable ligands. Curr Opin Neurobiol 2017. https://doi.org/10.1016/j. conb.2017.05.021.
- [33] Broichhagen J, Damijonaitis A, Levitz J, Sokol KR, Leippe P, Konrad D, Trauner D. Orthogonal optical control of a G protein-coupled receptor with a SNAP-tethered photochromic ligand. ACS Cent Sci 2015;1(7):383–93. https://doi.org/10.1021/acscentsci.5b00260
- [34] Donthamsetti PC, Broichhagen J, Vyklicky V, Stanley C, Fu Z, Visel M, Isacoff EY. Genetically-targeted optical control of an endogenous G protein-coupled receptor. J Am Chem Soc 2019. https://doi.org/10.1021/jacs.9b02895.
- [35] Farrants H, Gutzeit VA, Acosta-Ruiz A, Trauner D, Johnsson K, Levitz J, Broichhagen J. SNAP-tagged nanobodies enable reversible optical control of a G protein-coupled receptor via a remotely tethered photoswitchable ligand. ACS Chem Biol 2018;13(9):2682–8. https://doi.org/10.1021/acschembio.8b00628. research-article.
- [36] Levitz J, Broichhagen J, Leippe P, Konrad D, Trauner D, Isacoff EY. Dual optical control and mechanistic insights into photoswitchable group II and III metabotropic glutamate receptors. Proc Natl Acad Sci USA 2017;114(17): E3546–54. https://doi.org/10.1073/pnas.1619652114.
- [37] Polenghi A, Nieus T, Guazzi S, Gorostiza P, Petrini EM, Barberis A. Kainate receptor activation shapes short-term synaptic plasticity by controlling receptor lateral mobility at glutamatergic synapses. Cell Rep 2020;31(10):107735. https://doi.org/10.1016/j.celrep.2020.107735.
- [38] Reiner A, Isacoff EY. Tethered ligands reveal glutamate receptor desensitization depends on subunit occupancy. Nat Chem Biol 2014;(february):1–10. https://doi. org/10.1038/nchembio.1458.
- [39] Acosta-Ruiz A, Gutzeit VA, Skelly MJ, Meadows S, Lee J, Parekh P, Levitz J. Branched photoswitchable tethered ligands enable ultra-efficient optical control and detection of G protein-coupled receptors in vivo. Neuron 2020;105(3): 446–463,e13. https://doi.org/10.1016/j.neuron.2019.10.036.
- [40] Sandoz G, Levitz J, Kramer RH, Isacoff EY. Optical control of endogenous proteins with a photoswitchable conditional subunit reveals a role for TREK1 in GABA(B) signaling. Neuron 2012;74(6):1005–14. https://doi.org/10.1016/j. peuron 2012 04 026
- [41] Bregestovski P, Maleeva G, Gorostiza P. Light-induced regulation of ligand-gated channel activity. Br J Pharmacol 2018;175(11):1892–902. https://doi.org/ 10.1111/hph.14022
- [42] Castagna R, Kolarski D, Durand-de Cuttoli R, Maleeva G. Orthogonal control of neuronal circuits and behavior using photopharmacology. J Mol Neurosci 2022; 72(7):1433–42. https://doi.org/10.1007/s12031-022-02037-3.
- [43] Izquierdo-Serra M, Bautista-Barrufet A, Trapero A, Garrido-Charles A, Díaz-Tahoces A, Camarero N, Gorostiza P. Optical control of endogenous receptors and cellular excitability using targeted covalent photoswitches. Nat Commun 2016;7: 12221. https://doi.org/10.1038/ncomms12221.
- [44] Garrido-Charles A, Huet A, Matera C, Thirumalai A, Hernando J, Llebaria A, Gorostiza P. Fast photoswitchable molecular prosthetics control neuronal activity in the cochlea. J Am Chem Soc 2022. https://doi.org/10.1021/jacs.1c12314.
- [45] De Simoni A, Griesinger CB, Edwards FA. Development of rat CA1 neurones in acute versus organotypic slices: role of experience in synaptic morphology and activity. J Physiol 2003;550(Pt 1):135–47. https://doi.org/10.1113/ iphysiol.2003.039099.
- [46] Cabré G, Garrido-Charles A, Moreno M, Bosch M, Porta-de-la-Riva M, Krieg M, Alibés R. Rationally designed azobenzene photoswitches for efficient two-photon neuronal excitation. Nat Commun 2019;10(1). https://doi.org/10.1038/s41467-019-08796-9
- [47] Pittolo S, Lee H, Lladó A, Tosi S, Bosch M, Bardia L, Gorostiza P. Reversible silencing of endogenous receptors in intact brain tissue using 2-photon pharmacology. Proc Natl Acad Sci USA 2019;116(27):13680–9. https://doi.org/ 10.1073/pnas.1900430116.
- [48] Carroll RC, Lissin DV, von Zastrow M, Nicoll RA, Malenka RC. Rapid redistribution of glutamate receptors contributes to long-term depression in hippocampal cultures. Nat Neurosci 1999;2(5):454–60. https://doi.org/10.1038/ 8123.
- [49] Lüthi A, Chittajallu R, Duprat F, Palmer MJ, Benke TA, Kidd FL, Collingridge GL. Hippocampal LTD expression involves a pool of AMPARs regulated by the NSF-GluR2 interaction. Neuron 1999;24(2):389–99. https://doi.org/10.1016/s0896-6273(00)80852-1.

- [50] Lee HK, Kameyama K, Huganir RL, Bear MF. NMDA induces long-term synaptic depression and dephosphorylation of the GluR1 subunit of AMPA receptors in hippocampus. Neuron 1998;21(5):1151–62. https://doi.org/10.1016/S0896-6273(00)80632-7
- [51] Carotenuto R, Pallotta MM, Tussellino M, Fogliano C. Xenopus laevis (Daudin, 1802) as a model organism for bioscience: a historic review and perspective. Biology 2023;12(6). https://doi.org/10.3390/biology12060890.
- [52] Horb M, Wlizla M, Abu-Daya A, McNamara S, Gajdasik D, Igawa T, Guille M. Xenopus resources: transgenic, inbred and mutant animals, training opportunities, and web-based support. Front Physiol 2019;10:387. https://doi.org/10.3389/fphys.2019.00387.
- [53] Pittolo S, Gómez-Santacana X, Eckelt K, Rovira X, Dalton J, Goudet C, Gorostiza P. An allosteric modulator to control endogenous G protein-coupled receptors with light. Nat Chem Biol 2014;10(10):813–5. https://doi.org/ 10.1038/nchembio.1612.
- [54] Huang Y-B, Hu C-R, Zhang L, Yin W, Hu B. In vivo study of dynamics and stability of dendritic spines on olfactory bulb interneurons in Xenopus laevis tadpoles. PLoS One 2015;10(10):e0140752. https://doi.org/10.1371/journal. pone.0140752.
- [55] Falk J, Drinjakovic J, Leung KM, Dwivedy A, Regan AG, Piper M, Holt CE. Electroporation of cDNA/Morpholinos to targeted areas of embryonic CNS in xenopus. BMC Dev Biol 2007;7:107. https://doi.org/10.1186/1471-213X-7-107.
- [56] Wong HH-W, Holt CE. Targeted electroporation in the CNS in xenopus embryos. In: Vleminckx K, editor. Xenopus. Methods in molecular biology; 2018. p. 119–30. New York, NY.
- [57] Berlin S, Szobota S, Reiner A, Carroll EC, Kienzler MA, Guyon A, Isacoff EY. A family of photoswitchable NMDA receptors. eLife 2016:1–29. https://doi.org/ 10.7554/eLife 12040
- [58] Gorostiza P, Volgraf M, Numano R, Szobota S, Trauner D, Isacoff EY. Mechanisms of photoswitch conjugation and light activation of an ionotropic glutamate receptor. Proc Natl Acad Sci USA 2007;104(26):10865–70. https://doi.org/ 10.1073/pnas.0701274104.
- [59] Numano R, Szobota S, Lau AY, Gorostiza P, Volgraf M, Roux B, Isacoff EY. Nanosculpting reversed wavelength sensitivity into a photoswitchable iGluR. Proc Natl Acad Sci USA 2009;106(16):6814–9. https://doi.org/10.1073/pnas.0811899106.
- [60] Volgraf M, Gorostiza P, Numano R, Kramer RH, Isacoff EY, Trauner D. Allosteric control of an ionotropic glutamate receptor with an optical switch. Nat Chem Biol 2006;2(1):47–52. https://doi.org/10.1038/nchembio756.
- [61] Harvey JH, Trauner D. Regulating enzymatic activity with a photoswitchable affinity label. Chembiochem 2008;9(2):191–3. https://doi.org/10.1002/ chic 200700570
- [62] Takato M, Sakamoto S, Nonaka H, Tanimura Valor FY, Tamura T, Hamachi I. Photoproximity labeling of endogenous receptors in the live mouse brain in minutes. Nat Chem Biol 2024;21(January). https://doi.org/10.1038/s41589-024.01692.4
- [63] Barber DM, Liu S-A, Gottschling K, Sumser M, Hollmann M, Trauner D. Optical control of AMPA receptors using a photoswitchable quinoxaline-2,3-dione antagonist. Chem Sci 2017;8(1):611–5. https://doi.org/10.1039/C6SC01621A.
- [64] Gisela Cabré, Garrido-Charles A, González-Lafont À, Moormann W, Langbehn D, Egea D, Hernando J. Synthetic photoswitchable neurotransmitters based on bridged azobenzenes. Org Lett 2019. https://doi.org/10.1021/acs.org/ett/9h01222
- [65] Volgraf M, Gorostiza P, Szobota S, Helix MR, Isacoff EY, Trauner D. Reversibly caged glutamate: a photochromic agonist of ionotropic glutamate receptors. J Am Chem Soc 2007;129(2):260–1. https://doi.org/10.1021/ja067269o.
- [66] Durand-de Cuttoli R, Chauhan PS, Pétriz Reyes A, Faure P, Mourot A, Ellis-Davies GCR. Optofluidic control of rodent learning using cloaked caged glutamate. Proc Natl Acad Sci USA 2020;117(12):6831–5. https://doi.org/10.1073/nnas.1920869117
- [67] Noguchi J, Nagaoka A, Hayama T, Ucar H, Yagishita S, Takahashi N, Kasai H. Bidirectional in vivo structural dendritic spine plasticity revealed by two-photon glutamate uncaging in the mouse neocortex. Sci Rep 2019;9(1):1–8. https://doi. org/10.1038/s41598-019-50445-0.
- [68] Chambers JJ, Gouda H, Young DM, Kuntz ID, England PM. Photochemically knocking out glutamate receptors in vivo. J Am Chem Soc 2004;126(43): 13886–7. https://doi.org/10.1021/ja048331p.
- [69] Fino E, Araya R, Peterka DS, Salierno M, Etchenique R, Yuste R. RuBi-Glutamate: two-photon and visible-light photoactivation of neurons and dendritic spines. Front Neural Circ 2009;3(MAY):1–9. https://doi.org/10.3389/ neuro.04.002.2009.
- [70] Matsuzaki M, Ellis-Davies GCR, Nemoto T, Miyashita Y, Iino M, Kasai H. Dendritic spine geometry is critical for AMPA receptor expression in hippocampal CA1 pyramidal neurons. Nat Neurosci 2001;4(11):1086–92. https://doi.org/10.1038/ nn736.
- [71] Bosch M, Castro J, Saneyoshi T, Matsuno H, Sur M, Hayashi Y. Structural and molecular remodeling of dendritic spine substructures during long-term potentiation. Neuron 2014;86(12):3279–88. https://doi.org/10.1016/j. neuron.2014.03.021.
- [72] Noguchi J, Nagaoka A, Watanabe S, Ellis-Davies GCR, Kitamura K, Kano M, Kasai H. In vivo two-photon uncaging of glutamate revealing the structure-function relationships of dendritic spines in the neocortex of adult mice. J Physiol 2011;589(Pt 10):2447–57. https://doi.org/10.1113/jphysiol.2011.207100.
- [73] Cuttoli R D De, Mondoloni S, Marti F, Lemoine D, Nguyen C, Naudé J, Mourot A. Manipulating midbrain dopamine neurons and reward-related behaviors with

- light-controllable nicotinic acetylcholine receptors. eLife 2018;7:1–23. https://doi.org/10.7554/eLife.37487.
- [74] Wang D, Yu Z, Yan J, Xue F, Ren G, Jiang C, Yang X. Photolysis of Caged-GABA rapidly terminates seizures in vivo: concentration and light intensity dependence. Front Neurol 2017;8:215. https://doi.org/10.3389/fneur.2017.00215.
- [75] Cuttoli R D De, Chauhan PS, Reyes AP, Faure P, Mourot A, Ellis-Davies GCR. Optofluidic control of rodent learning using cloaked caged glutamate. Proc Natl Acad Sci USA 2020;117(12):6831–5. https://doi.org/10.1073/pnas.1920869117.
- [76] Oh WC, Hill TC, Zito K. Synapse-specific and size-dependent mechanisms of spine structural plasticity accompanying synaptic weakening. Proc Natl Acad Sci USA 2013;110(4):E305–12. https://doi.org/10.1073/pnas.1214705110.
- [77] Callaway EM, Katzt LC. Photostimulation using caged glutamate reveals functional circuitry in living brain slices. Proc Natl Acad Sci 1993;90:7661–5.
- [78] Cornejo VH, Ofer N, Yuste R. Voltage compartmentalization in dendritic spines in vivo. Science (New York, NY) 2022;375(6576):82–6. https://doi.org/10.1126/ science.abg0501.
- [79] Gobbo F, Marchetti L, Jacob A, Pinto B, Binini N, Pecoraro Bisogni F, Cattaneo A. Activity-dependent expression of Channelrhodopsin at neuronal synapses. Nat Commun 2017;8(1):1629. https://doi.org/10.1038/s41467-017-01699-7.
- [80] Packer AM, Peterka DS, Hirtz JJ, Prakash R, Deisseroth K, Yuste R. Two-photon optogenetics of dendritic spines and neural circuits. Nat Methods 2012;9(12): 1202–5. https://doi.org/10.1038/nmeth.2249.
- [81] Markram H, Gupta A, Uziel A, Wang Y, Tsodyks M. Information processing with frequency-dependent synaptic connections. Neurobiol Learn Mem 1998;70(1–2): 101–12. https://doi.org/10.1006/nlme.1998.3841.
- [82] Markram H, Wang Y, Tsodyks M. Differential signaling via the same axon of neocortical pyramidal neurons. Proc Natl Acad Sci USA 1998;95(9):5323–8. https://doi.org/10.1073/pnas.95.9.5323.
- [83] Shepherd JD, Huganir RL. The cell biology of synaptic plasticity: AMPA receptor trafficking. Annu Rev Cell Dev Biol 2007;23:613–43. https://doi.org/10.1146/ annurev.cellbio.23.090506.123516.
- [84] Carta M, Fievre S, Gorlewicz A, Mulle C. Kainate receptors in the hippocampus. Eur J Neurosci 2014;39:1835–44. https://doi.org/10.1111/ejn.12590.
- [85] Henley JM, Wilkinson KA. Synaptic AMPA receptor composition in development, plasticity and disease. Nat Rev Neurosci 2016;17(6):337–50. https://doi.org/ 10.1038/nrn.2016.37.
- [86] Pellegrini-Giampietro DE, Zukin RS, Bennett MV, Cho S, Pulsinelli WA. Switch in glutamate receptor subunit gene expression in CA1 subfield of hippocampus following global ischemia in rats. Proc Natl Acad Sci USA 1992;89(21): 10499–503. https://doi.org/10.1073/pnas.89.21.10499.
- [87] Pickard L, Noël J, Henley JM, Collingridge GL, Molnar E. Developmental changes in synaptic AMPA and NMDA receptor distribution and AMPA receptor subunit composition in living hippocampal neurons. J Neurosci: Off J Soc Neurosci 2000; 20(21):7922–31. https://doi.org/10.1523/JNEUROSCI.20-21-07922.2000.
- [88] Zinchenko VP, Dolgacheva LP, Tuleukhanov ST. Calcium-permeable AMPA and kainate receptors of GABAergic neurons. Biophysical Rev 2024;16(2):165–71. https://doi.org/10.1007/s12551-024-01184-8.
- [89] Leippe P, Koehler Leman J, Trauner D. Specificity and speed: tethered photopharmacology. Biochemistry 2017. https://doi.org/10.1021/acs. biochem.7b00687.
- [90] Heine M, Groc L, Frischknecht R, Béïque J-C, Lounis B, Rumbaugh G, Choquet D. Surface mobility of postsynaptic AMPARs tunes synaptic transmission. Science (New York, NY) 2008;320(5873):201–5. https://doi.org/10.1126/ science.1152089.
- [91] Opazo P, Sainlos M, Choquet D. Regulation of AMPA receptor surface diffusion by PSD-95 slots. Curr Opin Neurobiol 2012;22(3):453–60. https://doi.org/10.1016/ j.conb.2011.10.010.
- [92] Kiani AK, Pheby D, Henehan G, Brown R, Sieving P, Sykora P, Bertelli M. Ethical considerations regarding animal experimentation. J Prevent Med Hygiene 2022; 63(2 Suppl 3):E255–66. https://doi.org/10.15167/2421-4248/ jpmh2022.63.253.2768.
- [93] Hyoe RK, Robert J. A xenopus tadpole alternative model to study innate-like T cell-mediated anti-mycobacterial immunity. Dev Comp Immunol 2019;92:253–9. https://doi.org/10.1016/j.dci.2018.12.002.
- [94] Robert J, Cohen N. The genus xenopus as a multispecies model for evolutionary and comparative immunobiology of the 21st century. Dev Comp Immunol 2011; 35(9):916–23. https://doi.org/10.1016/j.dci.2011.01.014.
- [95] Paredes R, Ishibashi S, Borrill R, Robert J, Amaya E. Xenopus: an in vivo model for imaging the inflammatory response following injury and bacterial infection. Dev Biol 2015;408(2):213–28. https://doi.org/10.1016/j.ydbio.2015.03.008.
- [96] Banach M, Robert J. Tumor immunology viewed from alternative animal modelsthe xenopus story. Current Pathobiol Rep 2017;5(1):49–56. https://doi.org/ 10.1007/s40139-017-0125-y.
- [97] Cong L, Qin Z-F, Jing X-N, Yang L, Zhou J-M, Xu X-B. Xenopus laevis is a potential alternative model animal species to study reproductive toxicity of phytoestrogens. Aquat Toxicol 2006;77(3):250–6. https://doi.org/10.1016/j. aguatox.2005.12.014.
- [98] Sim HJ, Kim S-H, Myung K-J, Kwon T, Lee H-S, Park TJ. Xenopus: an alternative model system for identifying muco-active agents. PLoS One 2018;13(2): e0193310. https://doi.org/10.1371/journal.pone.0193310.
- [99] Shigeoka T, Jung H, Jung J, Turner-Bridger B, Ohk J, Lin JQ, Holt CE. Dynamic axonal translation in developing and mature visual circuits. Cell 2016;166(1): 181–92. https://doi.org/10.1016/j.cell.2016.05.029.
- [100] Wong HHW, Lin JQ, Ströhl F, Roque CG, Cioni JM, Cagnetta R, Holt CE. RNA docking and local translation regulate site-specific axon remodeling in vivo. Neuron 2017;95(4):852–868.e8. https://doi.org/10.1016/j.neuron.2017.07.016.

- [101] Kienzler MA, Reiner A, Trautman E, Yoo S, Trauner D, Isacoff EY. A red-shifted, fast-relaxing azobenzene photoswitch for visible light control of an ionotropic glutamate receptor. J Am Chem Soc 2013;135(47):17683–6. https://doi.org/10.1021/ia408104w.
- [102] Rullo A, Reiner A, Reiter A, Trauner D, Isacoff EY, Woolley GA. Long wavelength optical control of glutamate receptor ion channels using a tetra-ortho-substituted azobenzene derivative. Chem Commun (Cambridge, England) 2014;50(93): 14613–5. https://doi.org/10.1039/c4cc06612j.
- [103] Izquierdo-Serra M, Gascón-Moya M, Hirtz JJ, Pittolo S, Poskanzer KE, Ferrer E, Gorostiza P. Two-photon neuronal and astrocytic stimulation with azobenzenebased photoswitches. J Am Chem Soc 2014;136(24):8693–701. https://doi.org/ 10.1021/ja5026326.
- [104] Kellner S, Berlin S. Two-photon excitation of azobenzene photoswitches for synthetic optogenetics. Appl Sci 2020;10.
- [105] Riefolo F, Matera C, Garrido-Charles A, Gomila AMJ, Sortino R, Agnetta L, Gorostiza P. Optical control of cardiac function with a photoswitchable muscarinic agonist. J Am Chem Soc 2019;141:7628–763. https://doi.org/ 10.1021/jacs.9b03505.

- [106] Sortino R, Cunquero M, Castro-Olvera G, Gelabert R, Moreno M, Riefolo F, Gorostiza P. Three-photon infrared stimulation of endogenous neuroreceptors in vivo. Angew Chem 2023;62(51):e202311181. https://doi.org/10.1002/ anie 202311181
- [107] Kaech S, Banker G. Culturing hippocampal neurons. Nat Protoc 2006;1(5): 2406–15. https://doi.org/10.1038/nprot.2006.356.
- [108] Bosch M, Castro J, Sur M, Hayashi Y. Photomarking relocalization technique for correlated two-photon and electron microcopy imaging of single stimulated synapses. In: Poulopoulos A, editor. Synapse development: methods and protocols. New York, NY: Springer New York; 2017. p. 185–214. https://doi.org/ 10.1007/978-1-4939-6688-2_14.
- [109] Nieuwkoop PD, Faber J, editors. Normal table of Xenopus laevis (Daudin): a systematical and chronological survey of the development from the fertilized egg till the end of metamorphosis. New York: Garland Pub; 1994.
- [110] Schindelin J, Arganda-Carreras I, Frise E, Kaynig V, Longair M, Pietzsch T, Cardona A. Fiji: an open-source platform for biological-image analysis. Nat Methods 2012;9(7):676–82. https://doi.org/10.1038/nmeth.2019.